Theoretical Study for Chemical Processes in Solution Based on Statistical Mechanics of Molecular Liquids

原野, 雄一

(Degree)
博士（理学）

(Date of Degree)
2001-03-31

(Date of Publication)
2013-05-27

(Resource Type)
doctoral thesis

(Report Number)
甲2247

(URL)
https://hdl.handle.net/20.500.14094/D1002247

博士論文

Theoretical Study for Chemical Processes in Solution Based on Statistical Mechanics of Molecular Liquids

平成１３年１月

神戸大学大学院自然科学研究科

原野雄一

博士論文

Theoretical Study for Chemical Processes in Solution Based on Statistical Mechanics of Molecular Liquids

(分子性液体の統計力学に基づく溶液内化学過程の理論的研究)

平成１３年１月

神戸大学大学院自然科学研究科

原野雄一

Contents

Chapter 1

General Introduction

1.1 Statistical Mechanics of Molecular Liquids

When we consider that most chemical reactions take place in solution, evaluating "solvent effect" becomes the most important aspect in many fields including organic and biological chemistries.[1,2] Actually most of experiments in chemistry have been done in liquid state. Theoretical interpretations of such experimental data are essential in order to understand the "solvent effect".

In theoretical side, phenomenological models or continuum models represented by the Born model for the ion hydration,[3] Onsager's reaction field,[4] and the Stokes-Einstein-Debye law[5-7] for irreversible processes have long been standard concepts both in physics and chemistry of condensed matters. However, enormous varieties of molecules exist in the material world, and it is impossible to describe the properties of huge number of molecular species with making use of a few empirical parameters. Moreover, the latest development in the experimental techniques have revealed the serious break down of such models. In order for the theory to make sense to experimental chemistries, the theory of liquid and liquid mixture should be able to handle the huge varieties of molecules as an assembly of particles.

As we can observe so-called "Brownian molecular movement", molecules seem to be moving randomly in a liquid state, where the positions of each molecules in a moment are meaningless. However, interactions between molecules would restrict the movement of molecules to a certain extent. For description of the liquid state from the view point of

such a molecular aspect, correlation functions between particles; i.e., radial distribution functions have an essential importance. In order to obtain these properties based on statistical mechanics, the Ornstein-Zernike (OZ) integral equation was proposed.[8] However, it originally supposed for a spherical molecule and cannot handle the molecular geometry, which is essential for chemical characteristics. The major break though toward the molecular liquid theory has been made by Chandler and Andersen in 1971 with reference interaction site model (RISM) theory,[9,10] which is a extension of the OZ equation to a mixture of atoms but respects chemical bonds as strong intramolecular correlations. The RISM theory has been extended for molecule with charges, which plays a dominant role in determining the chemical specificity of the molecule.[11-16] The extended RISM theory has become one of the most powerful tools for investigating the liquid structure as a theme of chemistry. A brief outline of this theory, on which this study is mostly based, is given in the following.

1.2 Reference Interaction Site Model (RISM) for Molecular Liquids

The most significant characteristic of molecular liquid is that molecular interaction depends not only on the separation between them but also their orientations. The following model is representative one to describe that characteristic,

$$u(1,2) = u(R, \Omega_1, \Omega_2), \tag{1.1}$$

where R is the distance between the "center" or"origins" in the body fixed frame of molecules, and Ω_1 and Ω_2 mean the orientation of molecule "1" and "2". The contribution of the orientations can be alternatively expressed as the summation of interaction between the atoms composing the molecule,

$$u(1,2) = \sum_{\alpha,\gamma} u_{\alpha\gamma}(r), \tag{1.2}$$

where α and γ denote α atom of the molecule "1" and γ atom of the molecule "2". The summation is repeated for all atoms. This model is called "interaction site model"

(ISM) and equivalent to $u(1,2)$ when proper parameter is given for $u_{\alpha\gamma}(r)$. The molecular simulation usually employs this assumption.

1.2.1 Correlation Function of Polyatomic Molecules

Here, we consider a system of N particles in a volume V. The local density of atom type α at position $\mathbf{r}$ is defined with the Dirac δ-function,

$$\nu_\alpha(\mathbf{r}) = \sum_{i=1}^{N} \delta(\mathbf{r} - \mathbf{r}_i^\alpha), \tag{1.3}$$

and the thermal average of $\nu_\alpha(\mathbf{r})$ is identical to the density of of atom type α in uniform liquids,

$$\rho_\alpha(\mathbf{r}) = \langle \nu_\alpha(\mathbf{r}) \rangle. \tag{1.4}$$

It is the variance and covariance of the density fluctuation defined by

$$\chi_{\alpha\gamma}(\mathbf{r}, \mathbf{r}') = \langle (\nu_\alpha(\mathbf{r}) - \rho_\alpha(\mathbf{r}))(\nu_\gamma(\mathbf{r}') - \rho_\gamma(\mathbf{r}')) \rangle \tag{1.5}$$

that characterize the microscopic structure of the liquids.

Substituting Eqs. (1.3) and (1.4) for (1.5), and splitting the sum into intra-($i = j$) and inter-($i \neq j$) molecular contribution, Eq. (1.5) is rewritten as

$$\chi_{\alpha\gamma}(\mathbf{r}, \mathbf{r}') = \chi^{(0)}_{\alpha\gamma}(\mathbf{r}, \mathbf{r}') + \rho_\alpha(\mathbf{r})\rho_\gamma(\mathbf{r}')h_{\alpha\gamma}(\mathbf{r}, \mathbf{r}'), \tag{1.6}$$

where $\chi^{(0)}_{\alpha\gamma}(\mathbf{r}, \mathbf{r}')$ and $h_{\alpha\gamma}(\mathbf{r}, \mathbf{r}')$ respectively represent the intra and intermolecular correlation functions and are given by

$$\chi^{(0)}_{\alpha\gamma}(\mathbf{r}, \mathbf{r}') = \rho_\alpha(\mathbf{r})\delta(|\mathbf{r} - \mathbf{r}'|)\delta_{\alpha\gamma} + \rho_\alpha(\mathbf{r})s_{\alpha\gamma}(\mathbf{r}, \mathbf{r}'), \tag{1.7}$$

$$\rho_\alpha(\mathbf{r})\rho_\gamma(\mathbf{r}')h_{\alpha\gamma}(\mathbf{r}, \mathbf{r}') = \langle \sum_{i \neq j} \delta(\mathbf{r} - \mathbf{r}_i^\alpha)\delta(\mathbf{r}' - \mathbf{r}_j^\gamma) \rangle - \rho_\alpha(\mathbf{r})\rho_\gamma(\mathbf{r}'), \tag{1.8}$$

where $s_{\alpha\gamma}(\mathbf{r}, \mathbf{r}')$ is defined as

$$\rho_\alpha(\mathbf{r})s_{\alpha\gamma}(\mathbf{r}, \mathbf{r}') = \langle \sum_{i} \delta(\mathbf{r} - \mathbf{r}_i^\alpha)\delta(\mathbf{r}' - \mathbf{r}_i^\gamma) \rangle. \tag{1.9}$$

For a rigid molecule, with the distance $L_{\alpha\gamma}$ between α and γ sites, it holds the expression as

$$s_{\alpha\gamma}(\mathbf{r}, \mathbf{r}') = \frac{1}{4\pi L_{\alpha\gamma}^2}\delta(|\mathbf{r} - \mathbf{r}'| - L_{\alpha\gamma}). \tag{1.10}$$

1.2.2 The RISM Equation

It is convenient to use grand canonical ensemble[17] in which fluctuation of the number of particles are permitted. Consider an open system in which the particles interact via a pair potential $u(|\mathbf{r}-\mathbf{r}'|)$ and are subject to an external field Φ_{ext},

$$U = \sum u(|\mathbf{r}-\mathbf{r}'|) + \Phi_{\text{ext}}, \tag{1.11}$$

Φ_{ext} is defined as

$$\Phi_{\text{ext}} = \sum_{\alpha} \int d\mathbf{r}\rho_{\alpha}(\mathbf{r})\phi_{\alpha}(\mathbf{r}), \tag{1.12}$$

where $\phi_{\alpha}(\mathbf{r})$ is the external field to which the site α is subject at position $\mathbf{r}$. The grand canonical ensemble of the system (Ξ) is regarded as the functional of $\phi_{\alpha}(\mathbf{r})$, and, from the definition of a functional derivative, we obtain

$$\frac{\delta\Xi}{\delta[-\beta\phi_{\alpha}(\mathbf{r})]} = \rho_{\alpha}(\mathbf{r}), \tag{1.13}$$

$$\frac{\delta^2\Xi}{\delta[-\beta\phi_{\alpha}(\mathbf{r})]\delta[-\beta\phi_{\gamma}(\mathbf{r}')]} = \langle\nu_{\alpha}(\mathbf{r})\nu_{\gamma}(\mathbf{r}')\rangle - \rho_{\alpha}(\mathbf{r})\rho_{\gamma}(\mathbf{r}'), \tag{1.14}$$

where $\beta = 1/k_BT$, and from Eqs. (1.5), (1.13), (1.14),

$$\frac{\delta\rho_{\alpha}(\mathbf{r})}{\delta[-\beta\phi_{\gamma}(\mathbf{r}')]} = \chi_{\alpha\gamma}(\mathbf{r},\mathbf{r}'). \tag{1.15}$$

From Eq. (1.15), the direct correlation function ($\bar{c}_{\alpha\gamma}(\mathbf{r},\mathbf{r}')$) is defined as

$$\begin{aligned}\frac{\delta[-\beta\phi_{\alpha}(\mathbf{r})]}{\delta\rho_{\gamma}(\mathbf{r}')} &= \chi_{\alpha\gamma}(\mathbf{r},\mathbf{r}')^{-1} \\ &= \frac{\delta_{\alpha\gamma}\delta(\mathbf{r}-\mathbf{r}')}{\rho_{\alpha}(\mathbf{r})} - \bar{c}_{\alpha\gamma}(\mathbf{r},\mathbf{r}').\end{aligned} \tag{1.16}$$

In the same way, the intramolecular direct correlation function ($c^{(0)}_{\alpha\gamma}(\mathbf{r},\mathbf{r}')$) is defined as

$$\chi^{(0)}_{\alpha\gamma}(\mathbf{r},\mathbf{r}')^{-1} = \frac{\delta_{\alpha\gamma}\delta(\mathbf{r}-\mathbf{r}')}{\rho_{\alpha}(\mathbf{r})} - c^{(0)}_{\alpha\gamma}(\mathbf{r},\mathbf{r}'). \tag{1.17}$$

From Eq. (1.16), (1.17), we obtain

$$\frac{\delta[-\beta\phi_{\alpha}(\mathbf{r})]}{\delta\rho_{\gamma}(\mathbf{r}')} = \chi^{(0)}_{\alpha\gamma}(\mathbf{r},\mathbf{r}')^{-1} - (\bar{c}_{\alpha\gamma}(\mathbf{r},\mathbf{r}') - c^{(0)}_{\alpha\gamma}(\mathbf{r},\mathbf{r}')). \tag{1.18}$$

Substitute Eqs. (1.15) and (1.18) for the chain rule of the functional derivative,

$$\sum_{\eta}\int \frac{\delta\rho_{\alpha}(\mathbf{r})}{\delta[-\beta\phi_{\eta}(\mathbf{r}'')]}\frac{\delta[-\beta\phi_{\eta}(\mathbf{r}'')]}{\delta\rho_{\gamma}(\mathbf{r}')}d\mathbf{r}'' = \delta_{\alpha\gamma}\delta(\mathbf{r}-\mathbf{r}'), \tag{1.19}$$

and let Eqs. (1.6)~(1.8) be taken into account, the following integral equation of relation between $h_{\alpha\gamma}$ and $c_{\alpha\gamma}$ is obtained in uniform liquids ($\phi_\alpha(\mathbf{r}) = 0$).

$$\boldsymbol{\rho}\mathbf{h}\boldsymbol{\rho} = \boldsymbol{\omega} * \mathbf{c} * \boldsymbol{\omega} + \boldsymbol{\omega} * \mathbf{c} * \boldsymbol{\rho}\mathbf{h}\boldsymbol{\rho}, \tag{1.20}$$

where $*$ denotes the convolution integral, and $\boldsymbol{\rho}$ is the diagonal matrix of the uniform density. $\mathbf{h}$, $\mathbf{c}$, $\boldsymbol{\omega}$ are the matrices of which subscription indicates the intra and intermolecular atomic pair, and these elements are defined with Eq. (2.8) and the following Eqs.

$$c_{\alpha\gamma}(r) = \bar{c}_{\alpha\gamma}(r) - c^{(0)}_{\alpha\gamma}(r), \tag{1.21}$$

$$\omega_{\alpha\gamma}(r) = \chi^{(0)}_{\alpha\gamma}(r), \tag{1.22}$$

where r means the distance between the site α and γ. $h_{\alpha\gamma}$ and $c_{\alpha\gamma}$ are the total correlation function and the direct correlation function, respectively. The total correlation function is in relation to the radial distribution function ($g(r)$) as $h(r) = g(r) - 1$. Eq. (1.20) is usually called the RISM (Reference Interaction Site Model) integral equation. It is also called the SSOZ (Site-Site Ornstein-Zernike) equation since it can be regarded as the extension of the OZ equation for interaction sites. Actually, in the limit of zero or infinite for the bond length in the molecule, the RISM equation becomes identical to the OZ equation for simple liquids,

$$\mathbf{h} = \mathbf{c} + \mathbf{c} * \boldsymbol{\rho}\mathbf{h}. \tag{1.23}$$

Since the RISM equation contains the two unknown function h and c, another equation for h and c is necessary to obtain the solution. This equation is called "closure relation". The hypernetted-chain (HNC)[8] and Percus-Yevick (PY)[18,19] approximations are among the most popular ones.

$$\begin{aligned} c_{\alpha\gamma}(r) &= \exp[-\beta u_{\alpha\gamma}(r) + (h_{\alpha\gamma}(r) - c_{\alpha\gamma}(r))] \\ &\quad -1 - (h_{\alpha\gamma}(r) - c_{\alpha\gamma}(r)) \qquad \text{(HNC)}, \end{aligned} \tag{1.24}$$

$$\begin{aligned} c_{\alpha\gamma}(r) &= \exp[-\beta u_{\alpha\gamma}(r)](1 + (h_{\alpha\gamma}(r) - c_{\alpha\gamma}(r))) \\ &\quad -1 - (h_{\alpha\gamma}(r) - c_{\alpha\gamma}(r)) \qquad \text{(PY)}. \end{aligned} \tag{1.25}$$

These equations are obtained from omitting the specific diagram from the expansion of the pair correlation function with the Mayer's f-function ($f = \exp[-\beta u] - 1$).[8] The details of the approximation are not referred to here.

1.2.3 Extended RISM Theory

The electrostatic interactions between atoms, of which naive treatment causes divergence in the spatial integrals in the OZ type equations, has been handled by a renormalization technique originated by J. Mayer,[14] implemented in the OZ equations by Allnat, and fully explored by H.L. Friedman in their theories of the electrolyte solution. In that sense, the extended RISM theory[11-13] is also an natural extension of the Mayer-Allnat-Friedman electrolyte solution theory to the molecular liquids.

The RISM equation can be expressed with the direct correlation functions

$$\boldsymbol{\rho}\mathbf{h}\boldsymbol{\rho} = \boldsymbol{\omega} * \mathbf{c} * \boldsymbol{\omega} + \boldsymbol{\omega} * \mathbf{c} * \boldsymbol{\omega} * \mathbf{c} * \boldsymbol{\omega} + \cdots \tag{1.26}$$

With the expression of Rossky-Dale,[20] that is also written as

$$\mathbf{h} = \mathcal{C}[\mathbf{c}|\boldsymbol{\omega}], \tag{1.27}$$

where $\mathbf{t} = \mathbf{h} - \mathbf{c}$, and $\mathbf{t}$ is defined as

$$\mathbf{t} = \mathcal{C}[\mathbf{c}|\boldsymbol{\omega}] - \mathbf{c} \equiv \mathcal{C}'[\mathbf{c}|\boldsymbol{\omega}]. \tag{1.28}$$

Since the long-range asymptotics of the direct correlation function is equal to the interaction potential,

$$c_{\alpha\gamma}(r) \to -\beta\frac{z_\alpha z_\gamma}{r}. \tag{1.29}$$

This contribution causes the divergence in the spatial integrals. Therefore, $c(r)$ is divided into $\phi(r) \equiv -\beta z_\alpha z_\gamma / r$ and the remainder

$$c_s(r) = c(r) - \phi(r). \tag{1.30}$$

Then, Eq. (1.28) is written as

$$\begin{aligned} \mathbf{t} &= \mathcal{C}'[\mathbf{c_s} + \boldsymbol{\phi}|\boldsymbol{\omega}] \\ &= \mathcal{C}'[\boldsymbol{\phi}|\boldsymbol{\omega}] + \mathcal{C}'[\mathbf{c_s}|\boldsymbol{\omega} + \boldsymbol{\rho}\mathcal{C}[\boldsymbol{\phi}|\boldsymbol{\omega}]\boldsymbol{\rho}]. \end{aligned} \tag{1.31}$$

Furthermore, using the definition as

$$\mathbf{Q} = \mathcal{C}[\boldsymbol{\phi}|\boldsymbol{\omega}], \tag{1.32}$$

$$\mathbf{V} = \boldsymbol{\omega} + \boldsymbol{\rho}\mathbf{Q}\boldsymbol{\rho}, \tag{1.33}$$

Eq. (1.27) is expressed as

$$\mathbf{h} = C[\mathbf{c_s}|\mathbf{V}] + \mathbf{Q}, \tag{1.34}$$

where $\mathbf{Q}$ is the function which has the converging solution in the spatial integrals.

In addition, the closure relation should be also renormalized as well as the RISM equation and expressed as,

$$c_s = \exp[-\beta u + Q + \tau] - 1 - \tau - Q \qquad \text{(HNC)}, \tag{1.35}$$

$$c_s = \exp[-\beta u + Q](1 + \tau) - 1 - \tau - Q \qquad \text{(PY)}, \tag{1.36}$$

where τ is defined as

$$\tau = h - c - Q + \phi. \tag{1.37}$$

1.3 The Purpose of This Study

In this study, the recent topics in chemistry and biochemistry were investigated by using methods of the extended RISM theory, and the results are presented in the following two chapters.

In Chapter 2, solvent effects of ambient and supercritical water on a chemical reaction, which has been widely employed for the industrial production, are investigated by using the coupled method of the RISM theory and the molecular orbital theory.

In Chapter 3, a method calculating the partial molar volume, which has essential importance in pressure effects on chemical reaction, was developed. The method is applied to investigate the stability of biomolecule upon pressure.

Bibliography

[1] "Water in Biology, Chemistry and Physics," ed by G. W. Robinson, S. B. Zhu, S. Singh, and M.W. Evans, World Scientific, London (1996).

[2] C. Reichardt, in "Solvent and Solvent Effect in Organic Chemistry", VCH, Weinhein (1988).

[3] M. Born, *J. Phys.*, **1**, 45 (1920).

[4] L. Onsager, *J. Am. Chem. Soc.*, **58**, 1486 (1936).

[5] G. G. Stokes, *Trans. Cambridge Philos. Soc.*, **9**, 8 (1851).

[6] A. Einsten, "Investigation on the Theory of Brownian Movement" ed by R. Fruth, A. D. Cowper, Trans., Dover and New York (1956).

[7] P. Debye, " Polar Molcules", Chemical Catalog Company, New York (1929).

[8] (a) J. P. Hansen and I. R. McDonald,
"Theory of Simple Liquids - 2nd ed.", (Academic Press, New York, 1986).
(b) R. A. McQuarrie, "Statistical Mechanics", (Harper Collins, New York, 1973).

[9] D. Chandler and H. C. Andersen, *J. Chem. Phys.*, **57**, 1930 (1972).

[10] D. Chandler, *J. Chem. Phys.*, **59**, 2742 (1973).

[11] F. Hirata and P. J. Rossky, *Chem. Phys. Lett.*, **83**, 329 (1981).

[12] F. Hirata, B. M. Pettitt, and P. J. Rossky, *J. Chem. Phys.*, **77**, 509 (1982).

[13] F. Hirata, P. J. Rossky, and B. M. Pettitt, *J. Chem. Phys.*, **78**, 509 (1983).

[14] J. Mayer, *J. Chem. Phys.*, **18**, 1426 (1950).

[15] J. Perkyns and B. M. Pettitt, *Chem. Phys. Lett.*, **190**, 626 (1992).

[16] J. Perkyns and B. M. Pettitt, *J. Chem. Phys.*, **97**, 7656 (1992).

[17] D. Chandler, J. D. McCoy, and S. J. Singer, *J. Chem. Phys.*, **85**, 5971 (1986).

[18] J. K. Percus and G. J. Yevick, *Phys. Rev*, **110**, 1 (1958).

[19] G. Stell, *Physica*, **29**, 517 (1963).

[20] P. J. Rossky and W. D. T. Dale, *J. Chem. Phys.*, **73**, 2457 (1980).

Chapter 2

The Diels-Alder Reaction in Ambient and Supercritical Water

2.1 Introduction

The Diels-Alder reaction is a synthetic method which has been most widely employed for the production of polycyclic ring systems in organic chemistry. In the early 1980's, Breslow et al. showed that using water as solvent accelerates the Diels-Alder reaction dramatically.[1)] The observation has reversed the traditional notion that pericyclic reactions are insensitive to solvent effects. However, the low solubility of nonpolar solute in aqueous solvents restricts the choice of reagents, or requires special additives. In this regard, supercritical water (SCW)[2,3)] deserves attention due to its unique properties: it can dissolve a variety of solute, both polar and non-polar, depending on temperature and pressure. Recently, the Diels-Alder reactions in SCW, with several different diene/dienophile combinations, have been experimentally examined,[4)] and it was reported that SCW gives rise to higher yields compared to ambient water (AW), while extremely increasing the reaction rate. When it is compared with the usual organic solvent, SCW not only gives us higher yield and rate of the reaction but also provides further benefit concerned with the environmental protection: it is free from discharging harmful organic solvent into the environment. Thus, it is important to elucidate the mechanism of the reaction at molecular level, and to answer the questions: why is the reaction rate accelerated when the media is changed from organic solvent to AW and SCW, and why is the yield drastically

enhanced in SCW compared to AW?

Chemical reaction is undoubtedly the most important issue in the theoretical chemistry, and thus the electronic structure is a key to solve the problem. As long as molecules in the gas phase are concerned, the theory for the electronic structure has been established with its great success. However, when it comes to molecules in solution, the stage of theory is still an infant. Since it is actually impossible to solve the Schrödinger equation for entire system including about 10^{23} solvent molecules, the most promising approach so far is any type of hybrid between the classical solvent and quantum solute.

Theoretical studies of organic reactions in solution require descriptions for the electronic structure of molecules involved in the reaction and for solvent properties, which are closely coupled with each other. In the earlier work on a S_N2 reaction in SCW,[5-8] the continuum solvent model and the corresponding theory were applied. The method provides a reasonable account for the solvation free energy in terms of the agreement with experiments with respect to "number". The electronic structure and optimized geometry in SCW were also obtained. The approach has attracted people in the field, because it requires much less computational effort. The method, however, is not capable of providing any structural information for solvation, and thereby largely provides mismatches with the electronic structure theory in terms of the level of description. Moreover, the quantitative agreement with experiments itself should not be regarded as a great achievement, because the theory usually relies on a substantial number of adjustable parameters. Another method applied for the same reaction system is the molecular simulations.[9-11] The approaches have been very successful to account for the free energy change of solvation and its structure. However, their computational demands prevent one from evaluating the electronic structure of species involved in the reaction, which is subject to the field of solvent. Since change in the electronic structure is the primary cause of chemical reactions, the method has to overcome the high barrier to be applied to such problems.

As an alternative to those mentioned above, a new approach "RISM-SCF/MCSCF" has been proposed for calculating the electronic structure of a molecule in solution, which combines the integral equation theory of molecular liquids (RISM) and the *ab initio* molecular orbital theory (SCF/MCSCF).[12-14] The method determines self-consistently

the electronic structure of a solute and the solvent distribution around it. One of the advantages of our method is that it enables us to change easily thermodynamic conditions of the system, such as temperature and density. Thus, it is suitable for investigating the chemical reaction in solvent including SCW, which requires numerical analyses in wide range of temperature and pressure.[15)]

In this chapter, the Diels-Alder reactions in SCW as well as in AW were studied by means of the RISM-SCF/MCSCF method, and tried to answer the questions raised earlier in the section: why is the reaction rate accelerated when the media is changed from organic solvent to AW and SCW, and why is the yield drastically enhanced in SCW compared to AW? As a target system, the cycloaddition of cyclopentadiene (CP) with methyl vinyl ketone (MVK) was chosen, which has been well studied by experimental and theoretical approaches.[1,16-19)] The dienophile can take two different conformations, *s-cis* or *s-trans*, which may bind with the diene to make a transition structure in two possible conformations, *exo* or *endo*. Therefore, four possible combinations, *endo-cis*, *endo-trans*, *exo-cis* and *endo-trans*, are conceivable for the structure of transition state (TS). Previous *ab initio* calculations[20)] have shown that the endo-cis transition structure is of the lowest energy in several Diels-Alder reactions, but Assfeld et al. have shown in a recent calculation[23)] that the endo-trans transition structure becomes more stable in the reaction of CP and methyl acrylate in aqueous solution. Thus, calculations were performed for both the *endo-cis* and *endo-trans* reactions, and also examined which is the more stable transition structure for this reaction system in AW and SCW. The *exo* TS are not considered in this section since their energies are substantially greater than those of the *endo* TS in aqueous solution.[24)]

2.2 Methods

In this section, a brief outline of the RISM-SCF/MCSCF theory is given, which is employed in the present study to examine solvent effect on the Diels-Alder reactions in aqueous solutions.

The RISM-SCF/MCSCF theory consists of two major theoretical elements, the ab-

initio molecular orbital theory and the RISM integral equation method, which are combined together to determine self-consistently the electronic structure of a solute in solution and solvent distribution around the solute.

The RISM equations[32,33] for a solute-solvent system at infinite-dilution can be written as,

$$h_{vv} = \omega_v * c_{vv} * \omega_v + \rho \omega_v * c_{vv} * h_{vv}, \tag{2.1}$$

$$h_{uv} = \omega_u * c_{uv} * \omega_v + \rho w_u * c_{uv} * h_{vv}, \tag{2.2}$$

where the asterisk denote the spatial convolution integral, h and c stand for the site-site intermolecular pair correlation functions and the direct correlation functions, respectively, and ρ is the number density of solvent. The indices u and v denote the solute and solvent, respectively. The intramolecular correlation function ω defines the molecular geometry in terms of distance constraints,

$$\omega_{\alpha\gamma} = \delta_{\alpha\gamma}\delta(r) + (1 - \delta_{\alpha\gamma})s_{\alpha\gamma}(r), \tag{2.3}$$

where $\delta_{\alpha\gamma}$ is a Kronecker delta function and $s_{\alpha\gamma}$ is the intramolecular distribution function between the site α and γ belonging to the solute or solvent molecule. In this study, we used the hypernetted chain (HNC) closure relation of which usefulness is shown in the previous studies. It takes the following form in real space,

$$c_{\alpha\gamma}(r) = \exp[-\beta u_{\alpha\gamma}(r) + h_{\alpha\gamma}(r) - c_{\alpha\gamma}(r)] - [h_{\alpha\gamma}(r) - c_{\alpha\gamma}(r))] - 1, \tag{2.4}$$

where $\beta = 1/k_B T$, k_B is Boltzmann constant and $u_{\alpha\gamma}$ is the intermolecular interaction between sites α and γ. Here, we employ a usual (12-6-1) type potential function written as

$$u_{\alpha\gamma}(r) = u^{LJ}_{\alpha\gamma}(r) + q_\alpha q_\gamma / r, \tag{2.5}$$

$$u^{LJ}_{\alpha\gamma}(r) = 4\epsilon_{\alpha\gamma}\left[\left(\frac{\sigma_{\alpha\gamma}}{r}\right)^{12} - \left(\frac{\sigma_{\alpha\gamma}}{r}\right)^{6}\right], \tag{2.6}$$

where q_α is the partial charge on the site α, and $u^{LJ}_{\alpha\gamma}(r)$ is the Lennard-Jones (L-J) potential. $\epsilon_{\alpha\gamma}$ and $\sigma_{\alpha\gamma}$ are the usual L-J parameters for a pair of sites, α and γ. Prior

to the RISM-SCF cycle, the solvent correlation function h_{vv} is prepared by solving Eq. (2.1). Using h_{vv}, the solute-solvent pair correlation functions h_{uv} are obtained from Eq. (2.2).

In order to couple the solvent effects with the electronic structure of a solvated molecular system, total energy (E_{total}), which includes solute and solvent energy, is defined as,

$$E_{total} = E_{solute} + \delta\mu_{\mathrm{HNC}}, \tag{2.7}$$

where E_{solute} is the sum of electronic and nuclear repulsion energies, and can be estimated from *ab initio* electronic structure methods such as Hartree-Fock. $\delta\mu_{\mathrm{HNC}}$ is the excess chemical potential (or solvation free energy) derived by Chandler and Singer, and is calculated from the RISM equations with the HNC closure,[27]

$$\delta\mu = \frac{\rho}{2\beta}\sum_{\alpha\in u}\sum_{\gamma\in v}\int_0^\infty 4\pi r^2 dr(h_{\alpha\gamma}(r)^2 - 2c_{\alpha\gamma}(r) - h_{\alpha\gamma}(r)c_{\alpha\gamma}(r)). \tag{2.8}$$

E_{total} can be regarded as a functional of the molecular wave functions of solute, which are described in terms of molecular orbital (and CI coefficients, if necessary), as well as a functional of the site-density pair correlation functions in molecular liquid theory. A new operator for the electronic structure of a solvated molecule can be derived by variations with respect to these functions under the orthonormality constraints.[14]

$$\delta(E_{total} - [\text{constraint for orthonormality}]) = 0. \tag{2.9}$$

Prior to the RISM-SCF calculation, the usual ab initio MO calculations were executed and geometry for reactants, transition states (TS) and products were fully optimized in gas phase at restricted Hartree-Fock level by using double zeta (DZV) basis set.[25] The geometries of those were fixed for all the RISM-SCF calculations. Vibrational frequencies were calculated at the same level, and those having only one imaginary frequency were identified as TS by definition. For the calculation of the ideal terms in the Gibbs free energy of the solute molecules (F^{ideal}), the zero-point vibrational energy is taken into account. The imaginary frequency for transition states was ignored in calculations of the vibrational energy.

The total energy of the solute molecule in solvent and in gas phase was defined, respectively, by

$$F_{total,gas}(\text{solute}) = E_{elec,gas}(\text{solute}) + \Delta F^{ideal}(\text{solute}), \tag{2.10}$$

$$F_{total,solv}(\text{solute}) = E_{elec,solv}(\text{solute}) + \Delta F^{ideal}(\text{solute}) + \Delta\mu(\text{solute}), \tag{2.11}$$

where $E_{elec,gas}$ and $E_{elec,solv}$ represent the electronic energy of the solute in gas phase and in water, respectively. In solution, the electronic structure of the solute changes from that in gas phase due to the solute solvent interaction. The energy change of the electronic structure associated with solvation (ΔE_{re}) is defined as follows,

$$\Delta E_{re}(\text{solute}) = E_{elec,solv}(\text{solute}) - E_{elec,gas}(\text{solute}). \tag{2.12}$$

Regarding the potential functions for solute molecules, CH, CH_2 and CH_3 groups are treated as united-atoms, and the potential functions consist of the Lennard-Jones (L-J) and Coulomb interaction. The L-J parameters for the united atoms are taken from the OPLS.[21,22] However, all the L-J diameters used here are increased by 0.4 Å since RISM-SCF calculations for TSs did not converge. For transition states, these parameter were fixed at the same values as those of corresponding sites in the reactants. As a model for solvent water molecules, we employed a SPC-like model,[26] which has been successfully used in liquid state simulations. The temperature and density of the surrounding water we examined in this study were 298 K, 1.0 g/cm^3 for ambient condition and 873 K, 0.6 g/cm^3 for supercritical water. The reason why we have chosen the relatively high density of SCW is that the RISM method becomes less reliable when density is further decreased.

2.3 Energetics of the Diels-Alder Reaction in Aqueous Solution

2.3.1 Stabilization of the Transition State in Ambient Water.

The key results are shown in Figure 2.1 which exhibits the energy diagram for the reaction through the *endo-cis* transition structure in gas phase, in AW (298 K, 1.0 g/cm^3),

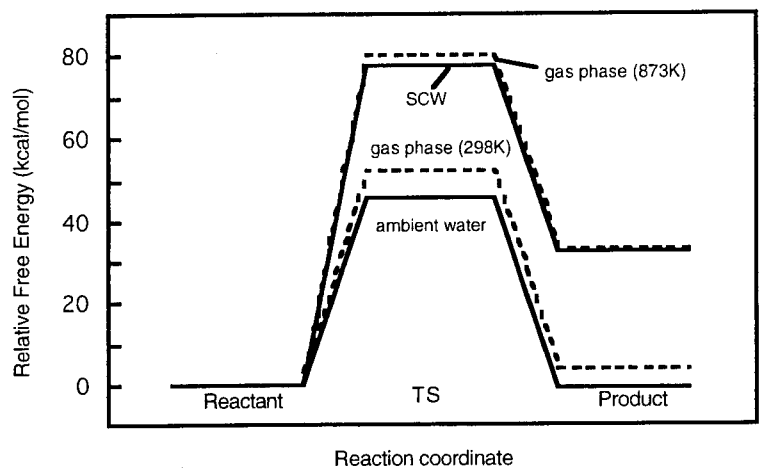

Figure 2.1: The total free energies of TS and the products relative to those of the reactants for the end-trans reaction.

and in SCW (873 K, 0.6 g/cm^3). All the energy levels are determined by regarding the reactants at corresponding temperature as a standard. The activation free energy ($\Delta F^{\ddagger}_{gas} = F_{total,gas}(\mathrm{TS}) - F_{total,gas}(\mathrm{reactants})$) computed in gas phase at 278 K is 52.48 kcal/mol. The $\Delta E^{\ddagger}_{AW}$ is calculated to be 45.58 kcal/mol: it is reduced by 6.90 kcal/mol from gas phase to AW (Table 2.1). This change originates essentially from the differences of the electrostatic reorganization energy ($\Delta E^{\ddagger}_{re} = \Delta E_{re}(\mathrm{TS}) - \Delta E_{re}(\mathrm{reactants})$) and the solvation free energy ($\Delta\mu^{\ddagger} = \Delta\mu(\mathrm{TS}) - \Delta\mu(\mathrm{reactants})$) between the reactant and TS. In Table 2.1, the change between these two energy contributions is compiled. As seen in the table, the stabilization of TS comes from a decrease in the solvation free energy associated with the reaction process from the reactant to TS, which includes geometrical change, giving rise to "desolvation" of water molecules at contact. The solvation free energy can be roughly decoupled into two contribution: the electrostatic and hydrophobic effects. In order to estimate the contribution of the hydrophobic effect, the geometry of the reactants was altered to that of TS, while charges on the sites were fixed. Consequently, the change of the solvation free energy comes from the loss of the water molecules contacting to the

Table 2.1: Changes in the activation free energy from gas phase to AW ($\Delta\Delta F^{\ddagger} = \Delta F^{\ddagger}_{AW} - \Delta F^{\ddagger}_{gas}$) and to SCW ($\Delta\Delta F^{\ddagger} = \Delta F^{\ddagger}_{SCW} - \Delta F^{\ddagger}_{gas}$)

	$\Delta\Delta F^{\ddagger}$	$\Delta\mu^{\ddagger}$	$\Delta E^{\ddagger}_{re}$
	AW		
trans	-7.54	-9.02	1.48
cis	-6.90	-10.98	4.09
	SCW		
trans	-3.40	-3.82	0.42
cis	-2.71	-3.43	0.72

(kcal/mol)

non-polar groups of the reactants and can be attributed to the hydrophobic effect. Then, the hydrophobic component is estimated to be -5.03 kcal/mol, which accounts for one half of $\Delta\mu^{\ddagger}$. However, this model possibly overestimates the hydrophobic component because the significant geometrical change may perturb the electronic structure of the solute and may remove the hydrogen-bonding to the carbonyl oxygen of reactant, MVK. These effect can give rise to some positive contribution to the hydrophobic component. On the basis of the analysis, other half of $\Delta\mu^{\ddagger}$ should come from the electrostatic effect including the hydrogen bonding around the carbonyl oxygen. Therefore, both the hydrophobic effect and the electrostatic effect contribute equally to the decrease in the solvation free energy.

Figure 2.2(a) shows the radial distribution functions (rdf's) of water oxygen and hydrogen around the carbonyl oxygen of MVK, TS, and product in AW. The height of the first peak of hydrogen's rdf's directly signifies the degree of hydrogen bonding. As shown in Figure 2.2(a), rdf's for the *endo-cis* reaction indicate that there is no significant change in height of the first peak when the reaction proceeds from the reactant to TS. At first glance, it appears that the hydrogen bonding is not enhanced. However, considering that a water molecule cannot access the carbonyl oxygen of TS geometrically more than to that of the reactant, MVK, the hydrogen bonding for TS must be stronger than that for the reactant, though the height of the first peak in rdf's does not change.

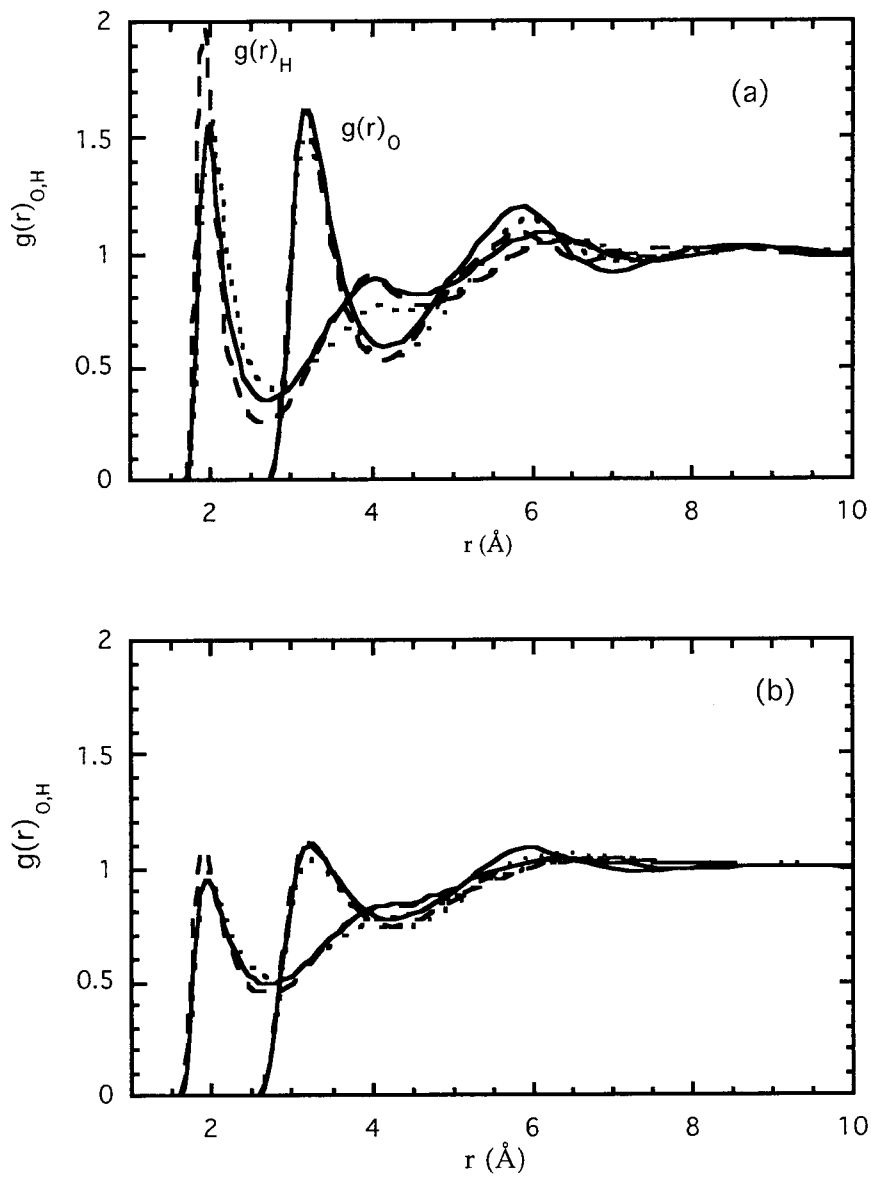

Figure 2.2: Radial distribution functions of water oxygen (g_O) and hydrogen (g_H) around the carbonyl oxygen of s-cis MVK (continuous line), endo-cis TS (dotted line) and endo-cis product (dashed line) in AW (a) and in SCW (b).

The (electronic) reorganization energy, ΔE_{re}, is increased by 4.09 kcal/mol in the reaction from the reactants to TS in case of the *endo-cis* reaction (Table 2.1). The more susceptive the solute molecule is to electrostatic effects, the more increased the reorganization energy is. In our case, electrostatic effects are attributed to hydration. Thus, hydration to the carbonyl group induces an increase in the reorganization energy. As the reactants reach TS, the reorganization energy is increased. This also supports the statement mentioned previously that hydrogen bonding is enhanced in TS compared to the reactant, MVK. Concerning the solvation free energy, both the hydrophobic effect and the electrostatic effect equally contribute to the stabilization of TS. At the same time, however, the enhanced hydrogen bonding for TS brings about an increase in the reorganization energy. The contribution of the hydrogen-bonding to $\Delta\Delta F^{\ddagger}$ is calculated to be -1.87 kcal/mol as a whole. Contribution of the reorganization energy to the activation energy, $\Delta E_{re}^{\ddagger}$, seems to compensate for the decrease of the solvation free energy due to the hydrogen bonding effect. Thus, the main contribution to the stabilization for the *endo-cis* TS can be attributed to the hydrophobic effect.

On the other hand, the estimated $\Delta F_{gas}^{\ddagger}$ is 54.25 kcal/mol at 298 K for the *endo-trans* reaction. Compared with the *endo-cis* reaction, it is higher by 1.77 kcal/mol. However, the activation free energy is reduced by 7.54 kcal/mol from gas phase to AW (Table 2.1). The value indicates that the *endo-trans* TS in AW is more stabilized than the *endo-cis* TS. By the component analysis for the solvation free energy described above, the hydrophobic component is calculated to be -4.99 kcal/mol, indicating that hydrophobic effect for stabilizing the endo-trans TS is essentially equal to the case for the *endo-cis* TS. The rest of the decrease in the solvation free energy can be attributed to the electrostatic effect. As seen in rdf's for the *end-trans* TS (Figure 2.3(a)), the hydrogen bonding is clearly enhanced compared to that for the reactant in contrast to the *endo-cis* case.

The electronic reorganization energy for the *endo-trans* TS is increased by 1.48 kcal/mol compared to that for the trans MVK. This value is much less than that for the *endo-cis* reaction. The total contribution of hydrogen-bonding effect including $\Delta E_{re}^{\ddagger}$ and $\Delta\mu^{\ddagger}$ is estimated as -2.55 kcal/mol. The result indicates that the hydrogen-bonding effect preferentially stabilizes the *endo-trans* TS more than the *endo-cis* TS. Therefore, the enhanced

hydrogen bonding effect, coupled with the electronic structure, is certainly an important factor to explain the degree of stabilization of TS, in contrast to the hydrophobic effect, which is almost constant.

The actual TS's would be determined by competition of two energy contributions: the electronic energy of an isolated molecule and the solvation free energy. The *endo-trans* TS has a greater dipole moment than the *endo-cis* TS in gas phase, and the difference in the dipole moment is enlarged in aqueous solution. Due to coupling of the dipole moment with solvent, the *endo-trans* TS gains greater energy of stabilization by 0.64 kcal/mol compared to the *endo-cis* TS. As long as the present reaction is concerned, the contribution from the electronic energy seems dominative over that from the solvation free energy. Consequently, the *endo-cis* TS is more stable than the *endo-trans* TS, thus, *endo-cis* reaction preferentially occurs. Those results, however, imply the existence of the Diels-Alder reactions, which may take place preferentially through the *endo-trans* TS in aqueous solution.

2.3.2 Mechanism of Rate Acceleration in Supercritical Water

The activation free energy, $\Delta F^{\ddagger}_{SCW}$, for the *endo-cis* reaction in SCW at 873.15 K is found to decrease by 2.71 kcal/mol compared with that in gas phase, $\Delta F^{\ddagger}_{gas}$. The degree of the stabilization in SCW, which is due to a decrease in the solvation free energy, is smaller than that in AW (Table 2.1). On the basis of the same analysis carried out in the previous section, contribution from the hydrophobic effect is 2.66 kcal/mol, which accounts for an 80% of decrease in the solvation free energy in SCW, 3.43 kcal/mol. The remaining 20% of $\Delta\mu^{\ddagger}$ comes from the hydrogen-bonding effect. As seen in Table 2.1, the increase in the electronic energy due to solvation, or the reorganization energy, in SCW is less than that in AW. In SCW, the electrostatic effects due to hydration become relatively small in comparison with the hydrophobic effect. Comparing the energy contribution of the hydrophobic effect with that of the hydrogen-bonding effect, both contributions reduce with the decreasing density of solvent water: the former reduces almost linearly and the latter drastically. The radial distribution functions in SCW shown in Figure 2.2(b) indicate that the hydrogen bonding is reduced drastically compared to that in AW.

The result also supports that the hydrogen-bonding effect is largely decreased in SCW. Furthermore, it was found that the general trend seen in AW applies to SCW as well; the activation free energy is decreased more in the endo-trans reaction. In SCW, the decrease in the free energy of the *endo-trans* TS is greater than that of the *endo-cis* TS by 0.69 kcal/mol (Table 2.1).

Concerning the electronic-structure change in TS, two different characters are conceivable: the "charge transferred (localized)" and "concerted (delocalized)" characters. In case of the *endo-cis reaction*, the charge in TS transferred from the diene to the dienophile in the gas phase is $0.1266|e|$, while that in AW is $0.2098|e|$. The results strongly suggest that contribution of the charge transfer mechanism is largely enhanced by the solvent effect in AW. The increase of the charge transfer in AW is thought to be due to hydrogen bonding around the carbonyl oxygen. The partial charge is found to be localized around the carbonyl group in TS. The charge transfer in SCW is less by $0.0408|e|$ than that in AW. By comparing the reaction in SCW to that in AW, it is found that the solvation effect in SCW becomes weaker than that in AW, although the substantial effect of solvent on the chemical reactions largely remains in SCW. These results seem quite reasonable if one considers that the density of water molecules in SCW is low and that the solvation effect in SCW is less than in AW. Thus, the mechanism of acceleration for the Diels-Alder reaction in SCW is considered to be different from that in AW.

The relative rate constant in AW and in SCW in the corresponding temperature could be roughly estimated from the activation energy on the basis of the simple transition state theory. The following analysis is performed concerning the reaction through the endo-cis TS. Suppose the rate of this reaction simply follows the Arrhenius equation, the relative rate constant is expressed as

$$k(T_1)/k(T_2) = \exp\{-(\Delta F(T_1)/RT_1 - \Delta F(T_2)/RT_2)\}. \tag{2.13}$$

It should be noted that Eq. (2.13) depends on an assumption that the prefactor in the rate expression, $k = \kappa \exp(-\Delta E^{\ddagger}/RT)$, is independent of temperature. The rate constants in AW and in SCW are, respectively, 1.14×10^6 and 4.76 times greater than those in gas phase at the corresponding temperature due to stabilization of the transition state by solvent. The accelerations are caused by the solvent effect as mentioned in previous paragraph.

The estimated rate of the reaction in gas phase at 873 K is 3.03×10^{19} times greater than that at 298 K. From these values, the relative rate constant in SCW compared to that in AW is estimated to be 1.27×10^{13}; the rate constant in SCW is extremely increased. Although the solvation effect for the rate constant is appearently decreased in SCW, the rate is dramatically increased because of the thermal activation rather than the solvation effect.

2.3.3 Physical Origin of the High Yield in Supercritical Water

To compare the yield of the reaction in SCW to that in AW, the following analysis is performed for the *endo-cis* reaction. The yields of a reaction in an experimental system are determined not only by the equilibrium constant but also by the solubility of the reactants in solvent, because undissolved molecules can not participate in the reaction. Therefore, we define an effective yield constant (K_{eff}) by a product of the Henry's law constant of the reactants (K_H) and the equilibrium constant of the reaction (K) as

$$K_{eff} = K_H \cdot K. \tag{2.14}$$

The Henry's law constant is obtained from the solvation free energy of the solute molecule dissolved into the solvent from the gas phase,

$$K_H = \exp(-\Delta\mu/RT). \tag{2.15}$$

The equilibrium constant K is related to the free energy difference between the reactant and the product ($\Delta F^{\phi} = F_{total}(\text{product}) - F_{total}(\text{reactnats})$) in the solvent,

$$K = \exp(-\Delta F^{\phi}/RT). \tag{2.16}$$

As is listed in Table 2.2, the product in AW is stabilized more than the reactant in terms of the both energy components: ($\Delta\mu^{\phi} = \Delta\mu(\text{product}) - \Delta\mu(\text{reactants})$) and the reorganization energy ($\Delta E_{re}^{\phi} = \Delta E_{re}(\text{product}) - \Delta\text{E}_{\text{re}}(\text{reactants})$). In case of the *endo-cis* product, the decrease in $\Delta\mu^{\phi}$ and ΔE_{re}^{ϕ} is -5.91 kcal/mol and 0.85 kcal/mol, respectively. From the same analysis carried out in TS, the hydrophobic component of the stabilization for the product is -4.23 kcal/mol, which accounts for 70% of the solvation free energy.

Table 2.2: Changes in the free energy of the reaction from gas phase to AW ($\Delta\Delta F^{\phi} = \Delta F^{\phi}_{AW} - \Delta F^{\phi}_{gas}$) and to SCW ($\Delta\Delta F^{\phi} = \Delta F^{\phi}_{SCW} - \Delta F^{\phi}_{gas}$)

	$\Delta\Delta F^{\phi}$	$\Delta\mu^{\phi}$	ΔE^{ϕ}_{re}
	AW		
trans	-3.63	-4.10	0.47
cis	-5.06	-5.91	0.85
	SCW		
trans	-0.87	-0.95	0.08
cis	-1.02	-1.13	0.11

(kcal/mol)

Compared to the case of TS (Table 2.1), changes in the reorganization energy in AW are relatively small, indicating that electrons in the product molecule are delocalized more than those in TS. As seen in Figure 2.3(a), the hydrogen bonding around the carbonyl oxygen is certainly enhanced in the product. However, the hydrogen bonding effect gives rise to -0.83 kcal/mol, and it barely contributes to stabilize the product molecule: the hydrogen-bonding effect contributes to the stabilization of the product much less than the hydrophobic effect.

The total decrease in the free energy of the reaction in SCW is -1.02 kcal/mol. Solvation effects are weaker in SCW than those in AW: both the decrease in the solvation free energy and the increase in the reorganization energy are less. The hydrophobic component changes from -4.23 to -1.04 kcal/mol, although it accounts for most of $\Delta\mu^{\phi}$ in SCW, -1.13 kcal/mol. The hydrogen-bonding effect is 0.02 kcal/mol and never contributes to the stabilization of the product molecule. As seen in Figure 2.1, the energies of TS and the product in SCW are greatly increased compared to those in AW. The Diels-Alder reaction is the one in which two molecules are combined into one by creating two C-C bonds. When the reaction proceeds, the entropy of the system becomes smaller as a matter of course. Thus, the Gibbs free energy difference between the isolated reactant and product molecules is enlarged under the high temperature condition. When the reaction goes through the endo-cis TS only, the equilibrium constant in AW and in SCW

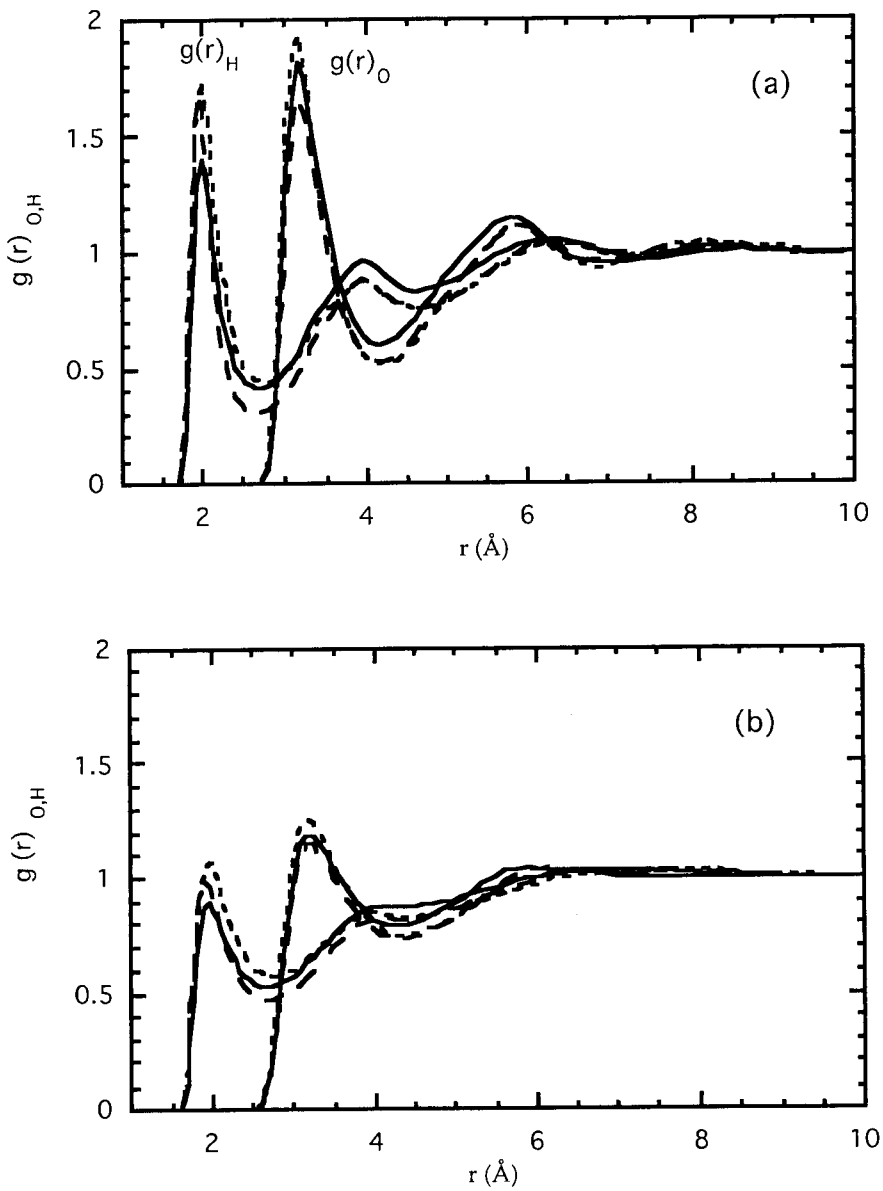

Figure 2.3: Radial distribution functions of water oxygen (g_O) and hydrogen (g_H) around the carbonyl oxygen of s-trans MVK (continuous line), endo-trans TS (dotted line) and endo-trans product (dashed line) in AW (a) and in SCW (b).

is calculated to be 6.27×10^7 and 0.20, respectively. Therefore, if the yield is determined thoroughly by the equilibrium constant of the reaction, the yield in SCW can never be higher than that in the AW. That is not the case in the experimental results. The solvation free energy of the reactants, CP and MVK, in AW were respectively calculated to be 19.68 kcal/mol and 11.04 kcal/mol, and those in SCW were 25.48 kcal/mol and 20.05 kcal/mol, respectively. Then, K_H in SCW is estimated to be 2.08×10^{11} times greater than that in AW, taking corresponding temperatures into account. On the basis of our definition of the effective yield constant, the yield in SCW is approximately 667 times higher than in AW. Our calculation shows that the energetics of the reaction in SCW gives a disadvantage regarding the yield, but the increased solubility of the reactants in solvent provides an advantage that is enough to overwhelm the energetical disadvantage.

2.3.4 Conclusion

In the this section, a theoretical study for a Diels-Alder reaction in gas phase, in ambient water (AW), and in supercritical water (SCW) are presented based on the RISM-SCF/MCSCF method, a combined *ab initio* electronic structure theory and the statistical mechanics of molecular liquids. We draw the following conclusions from the study.

The reaction rate in AW is increased largely in comparison with that in gas phase through reduced activation barrier due to the hydrophobic interaction. The reaction in SCW is accelerated due to increased thermal activation, not by the same cause in AW. The reaction yield is increased dramatically in SCW due to enhanced solubility compared to that in water.

Regarding Diels-Alder reactions, stereo-chemistry is another important issue studied by many authors. It has been observed experimentally that the endo/exo stereo-selectivity of products of the reaction becomes much higher in AW than that in organic solvents, and the selectivity disappears in SCW. It will be of great interest to see microscopically why water enhances the stereo-selectivity and why it disappears in SCW. Study along this line is presented in the next section.

2.4 Stereoselectivity for the Diels-Alder Reaction

It has been observed experimentally that the *endo/exo* stereo-selectivity of products of the reaction becomes much higher in AW than that in organic solvents, and that the selectivity disappears in SCW.[4,24] In this section, another important aspect of the reaction, stereo-chemistry, are also examined based on the RISM-SCF/MCSCF theory.

One of the most important achievements in the theoretical chemistry during the past century is the "frontier orbital theory" due to Fukui, which with the Woodward-Hoffmann rule, elucidated the special role played by so called "frontier orbitals" in the chemical reactions.[30,31] According to the theory, interactions between electrons in the highest occupied molecular orbital (HOMO) in one of the reactant species and those in the lowest unoccupied molecular orbitals (LUMO) in the other species determine essentially the chemical reactivity. The theory has provided a solid foundation in terms of quantum mechanics to the empirical "organic electronic theory", which has been popularly practiced among chemists for long time to predict reactivity and reaction path of organic compounds. The theory has been successfully applied not only to reactions caused by the electrostatic interaction between reactants, such as the nucleo- and electrophilic reactions, but also to those between neutral species, represented by the cycloaddition reactions. An advantage of the theory is to maintain the heuristic aspect of the "organic electronic theory" without sacrificing the quantum description of the electronic structure too much. It will be, therefore, beneficial for organic chemistry if one could explain solvent effects on organic reactions in terms of changes in the frontier orbitals due to solvent fields. In this section, the solvent effect on the *endo/exo* stereo-selectivity of cycloaddition reactions are examined in the light of the frontier orbital theory.

The cycloaddition of CP with MVK (Figure 2.4) was the first system to have been reported for the rate acceleration and the product selectivity and has been well studied by both experimental and theoretical approaches in AW. The dienophile can take two different conformations; *s-cis* or *s-trans*, which may bind with the diene to make a transition structure in two possible conformations; *exo* or *endo*. Therefore, four possible structures, *endo-cis*, *endo-trans*, *exo-cis* and *endo-trans*, are conceivable for the transition state (TS).

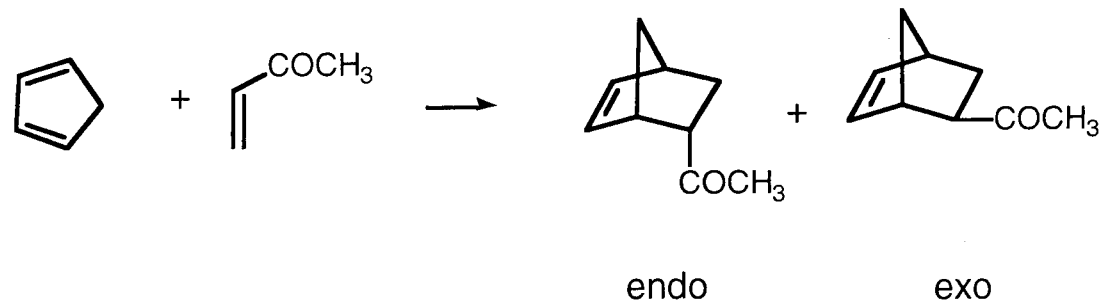

Figure 2.4: Scheme of the reaction system studied

Previous *ab initio* calculations[20] have shown that the *endo-cis* transition structure is of the lowest energy in several Diels-Alder reactions, but it has been reported in a recent calculation[23] that the *endo-trans* transition structure becomes more stable in the reaction of CP and methyl acrylate in aqueous solution. Thus, the calculations were performed on both *endo-cis* and *endo-trans* reaction, and *endo-cis* reaction was confirmed that it obtains the more stable transition structure for this reaction system both in AW and SCW. In the present study, the stereo-selectivity was examined only for the reaction through *cis* type transition structure.

2.4.1 Solvent Effect on the Reaction Energetics and Electronic Structure

In this section, the computational results of the solvent effect on the Diels-Alder reaction are first analyzed. Then, dependence of the *endo/exo* ratio of the reaction rate and the yield upon thermodynamic conditions is discussed. To get physical insight for the solvation effect on the reaction, a simple argument due to the frontier orbital theory is given. The *endo/exo* stereoselectivity of the Diels-Alder reaction has been well explained based on the Woodward-Hoffmann rule, in which the "secondary orbital interaction effect" in the HOMO-LUMO plays a crucial role to the observed *endo* preference.[31] It is, thus, of interest to view this modern computational results in terms of the frontier orbitals theory.

The total free energy of the solute molecule in solvent and in gas phase are respectively

defined by

$$F_{gas}^{total} = E_{gas}^{elec} + G_{id}, \tag{2.17}$$

and,

$$F_{solv}^{total} = E_{solv}^{elec} + G_{id} + \delta\mu, \tag{2.18}$$

where E_{gas}^{elec} and E_{solv}^{elec} represent the electronic energy of the solute in gas phase and in water, respectively. Here, we assume that the ideal Gibbs free energy for solute (G_{id}) does not change when it is transferred from gas into solvent. In solution, the electronic structure of the solute changes from that in gas phase due to the solute-solvent interaction. The energy change of the electronic structure due to solvation (δE_{re}) is defined by:

$$\delta E_{re} = E_{solv}^{elec} - E_{gas}^{elec}. \tag{2.19}$$

The solvation free energy $\delta\mu$ can be further decomposed into two contributions which represent hydrophobic (δF_{HP}) and hydrogen-bonding (δF_{HB}) interaction by the procedure described in the previous section.

$$\delta\mu = \delta F_{HP} + \delta F_{HB}. \tag{2.20}$$

Thus the total energy of a solvated molecule is expressed as

$$F_{solv}^{total} = E_{gas}^{elec} + G_{id} + \delta F_{HP} + \delta E_{re} + \delta F_{HB}, \tag{2.21}$$

where the last two terms represent the free energy change due to the electrostatic interaction including the distortion energy of electron clouds in the solute molecule.

The activation free energy ($\Delta F^{\ddagger}$) and the free energy change for the reaction (ΔF^{ϕ}) are defined by

$$\Delta F^{\ddagger} = F^{total}(TS) - F^{total}(reactant), \tag{2.22}$$

$$\Delta F^{\phi} = F^{total}(product) - F^{total}(reactant), \tag{2.23}$$

where $F^{total}(reactant)$ and $F^{total}(product)$ are the total free energies of the reactant and the product, and $F^{total}(TS)$ is that of the transition state. With the further decoupling

scheme mentioned above, the energy change due to solvent effect can be described as follows:

$$\delta\Delta F^{\ddagger/\phi} = \Delta F^{\ddagger/\phi}_{solv} - \Delta F^{\ddagger/\phi}_{gas} = \delta\Delta E^{\ddagger/\phi}_{re} + \delta\Delta F^{\ddagger/\phi}_{HB} + \delta\Delta F^{\ddagger/\phi}_{HP}. \tag{2.24}$$

Throughout this section, "δ" was used for changes of the quantities associated with solvation process and "Δ" for changes due to the reaction.

In Tables 2.3 and 2.4, the computed energy changes and their components are shown. Temperature and density of the surrounding water are 298.15 K, 1.0 g/cm^{3}for ambient condition (AW) and 873.15 K, 0.6 g/cm^{3}for supercritical condition (SCW). The theoretical results for the activation free energies ($\Delta F^{\ddagger}_{gas}$) at 298.15 K in gas phase are 52.48 kcal/moland 52.64 kcal/mol, respectively, for (*endo*) and (*exo*) TSs. They are very close each other but the *endo* TS is slightly lower in energy than the *exo* TS (0.16 kcal/mol). The activation free energy ($\Delta F^{\ddagger}_{AW}$) through the *endo* TS is reduced by 6.90 kcal/molin AW, but unfortunately the RISM-SCF calculation for the *exo* TS was not converged, and therefore the energy preference of TS in AW is unknown. The hydrophobic effect and the electrostatic effect (hydrogen bonding) equally contribute to the decrease of the solvation free energy for the *endo* TS as shown in the table. For the present case, the electrostatic effects are mainly due to the hydration of the CO group as clarified later. The activation free energies in SCW ($\Delta F^{\ddagger}_{SCW}$) are found to decrease by 2.71 kcal/mol(*endo*) and 2.25 kcal/mol(*exo*) compared with those in gas phase at 873.15 K. Both $\delta\Delta E_{re}$ and $\delta\Delta F_{HB}$ in SCW are less than those in AW, and the stabilization in SCW is attributed to the hydrophobic interaction ($\delta\Delta F_{HP}$). However, the solvent effect in SCW is smaller and about a half of that in AW. The total free energy of the *endo* isomer is lower than that of the *exo* one, and energy difference (0.16+0.46=0.62 kcal/mol) between the *endo* and *exo* isomers is slightly greater than that in gas phase. The product molecule is stabilized in AW more than the reactant with respect to all the energy components: $\delta\Delta F_{HP}$, $\delta\Delta F_{HB}$ and $\delta\Delta E_{re}$. Among them, the hydrophobic component ($\delta\Delta F_{HP}$) is predominant and accounts for about 60% of the total solvation effect. In SCW, solvation effects become much weaker but gives rise to decrease in all the energy components.

It should be noted that the preceding discussion concerns two aspects in the solvation effect: one is the energy lowering of TSs and/or products due to solvation, and the other

Table 2.3: The activation free energy and the free energy change for the reaction[a]

	Activation Free Energy			The Free Energy Change for Reaction		
	$\Delta E_{gas}^{elec\ddagger}$	$\Delta G_{id}^{\ddagger\ b}$	$\Delta F_{gas}^{\ddagger\ b}$	$\Delta E_{gas}^{elec\phi}$	$\Delta G_{id}^{\phi\ b}$	$\Delta F_{gas}^{\phi\ b}$
endo	37.17	15.31	52.48	-14.80	18.96	4.16
exo	37.15	15.49	52.64	-15.34	19.25	3.91

[a]given in kcal/mol [b] values at 298.15 K

Total energy of cis-MVK is -229.73961 and of CP is -192.73688 hartree.

Table 2.4: Free Energy Components of Solvent Effect in Diels-Alder Reaction

	$\delta\Delta F^{\ddagger}$				$\delta\Delta F^{\phi}$			
	AW		SCW		AW		SCW	
	endo	*exo*	*endo*	*exo*	*endo*	*exo*	*endo*	*exo*
$\delta\Delta F_{HP}$	-5.03	—	-2.66	-1.90	-4.23	-2.43	-1.04	-1.02
$\delta\Delta F_{HB}$	-5.95	—	-0.77	-1.00	-1.68	-1.64	-0.09	-0.01
$\delta\Delta E_{re}$	4.09	—	0.72	0.65	0.85	0.42	0.11	0.06
$\delta\Delta F^{\ddagger/\phi}$	-6.90	—	-2.71	-2.25	-5.06	-3.65	-1.02	-0.97

given in kcal/mol

Table 2.5: Dipole Moment, Effective Charge in the Dienophile on the Transition States

transition state	dipole moment[a]	effective charge[b]
	gas phase	
endo	4.00	-0.127
exo	3.19	-0.118
	AW	
endo	6.73	-0.210
exo	—	—
	SCW	
endo	5.48	-0.169
exo	4.52	-0.160

[a]In Debye, [b]In atomic units

is the enlarging of *endo-exo* energy difference that is concerned with the stereoselectivity. To help understanding these aspects, values of the dipole moment and of the effective charges assigned to the dienophile in TS are given in Table 2.5. We observe that the *endo* TS has greater dipole moment than the *exo* one, which can be explained as follows. The dipole moment of the isolated cis-MVK is computed to be 3.38 Debye, pointing the O→C direction. On the other hand, CP has a small dipole moment, 0.75 Debye, pointing toward the methylene groups along the C_{2v} axis (Figure 2.5). The relative directions of these dipole moments in the *endo* TS are parallel, giving rise to a higher overall dipole moment, while those in the *exo* TS are opposite and weaken each other. The dipole moment of the TSs is largely determined by the CO group with a small contribution from the approaching CP molecule. In AW, the dipole moment of the *endo* TS is enlarged to 6.73 Debye, while in SCW those for the *endo* and *exo* TSs are 5.48 Debye and 4.52 Debye, respectively.

The modification in the reaction energetics and the enhancement of polarization in the CO group upon solvation may be explained in terms of solvent effect on the frontier orbital energies (eigen values). In gas phase, the energy difference between the diene (CP) HOMO and the dienophile (MVK) LUMO (0.3884 hartree) is smaller than that between

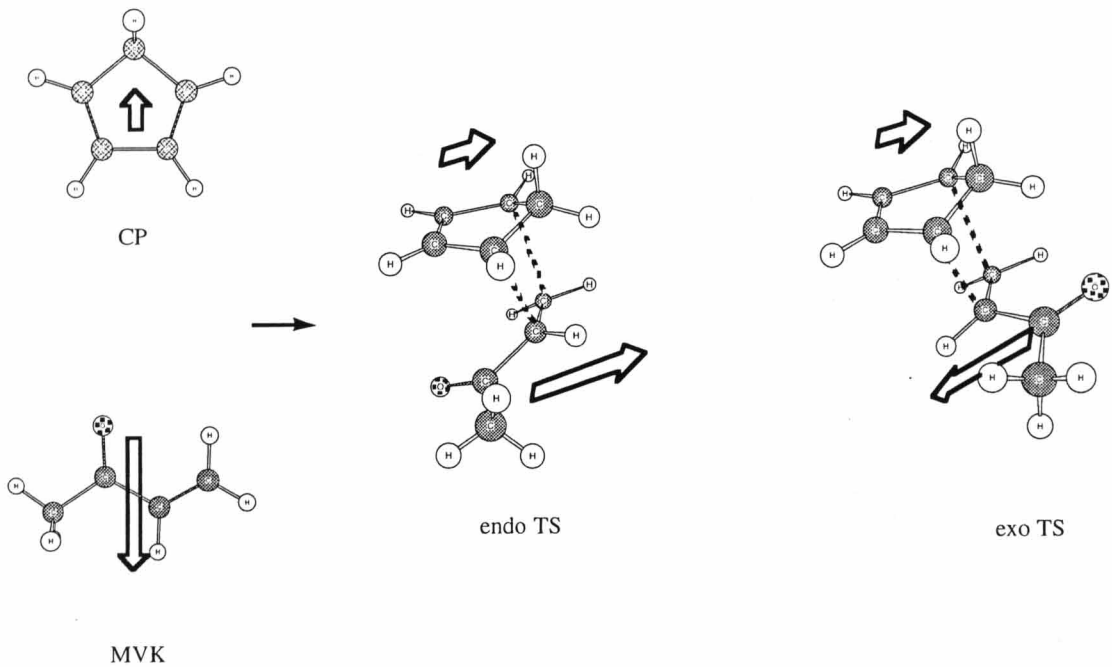

Figure 2.5: Illustration of the dipole moments in the reactant and the TSs.

the diene LUMO and the dienophile HOMO (0.5105 hartree), suggesting the former type of charge transfer interaction is more important (Figure 2.6(a)). Actually, the effective charges shown in the table indicate that the electron is localized at the MVK side in the TS. In case of the reaction in AW (Figure 2.6(b)), the energy difference between the diene HOMO and the dienophile LUMO is decreased to 0.3884 hartree, while the energy difference between the diene LUMO and dienophile HOMO is increased to 0.5105 hartree. The energy gaps in SCW are intermediate between those in gas phase and in AW, and computed to be 0.3845 and 0.5133 hartree (Figure 2.6(c)). The narrowing of the HOMO-LUMO energy gap should make the charge transfer interaction between the orbitals greater. The generated electronic structure which is polarized more compared to gas phase causes stabilization of TS due to the solute-solvent interaction. These are consistent with the effective charge assigned to the MVK in TS shown in Table 2.5. The charge assigned to the *endo* TS (-0.127) in gas phase is negative and slightly larger in magnitude than that of *exo* (-0.118). The charge in AW is calculated to be -0.210, strongly suggesting that the charge transfer interaction is largely enhanced by solvent effect in AW as is expected from the HOMO-LUMO energy gap. In SCW, the effective charges are

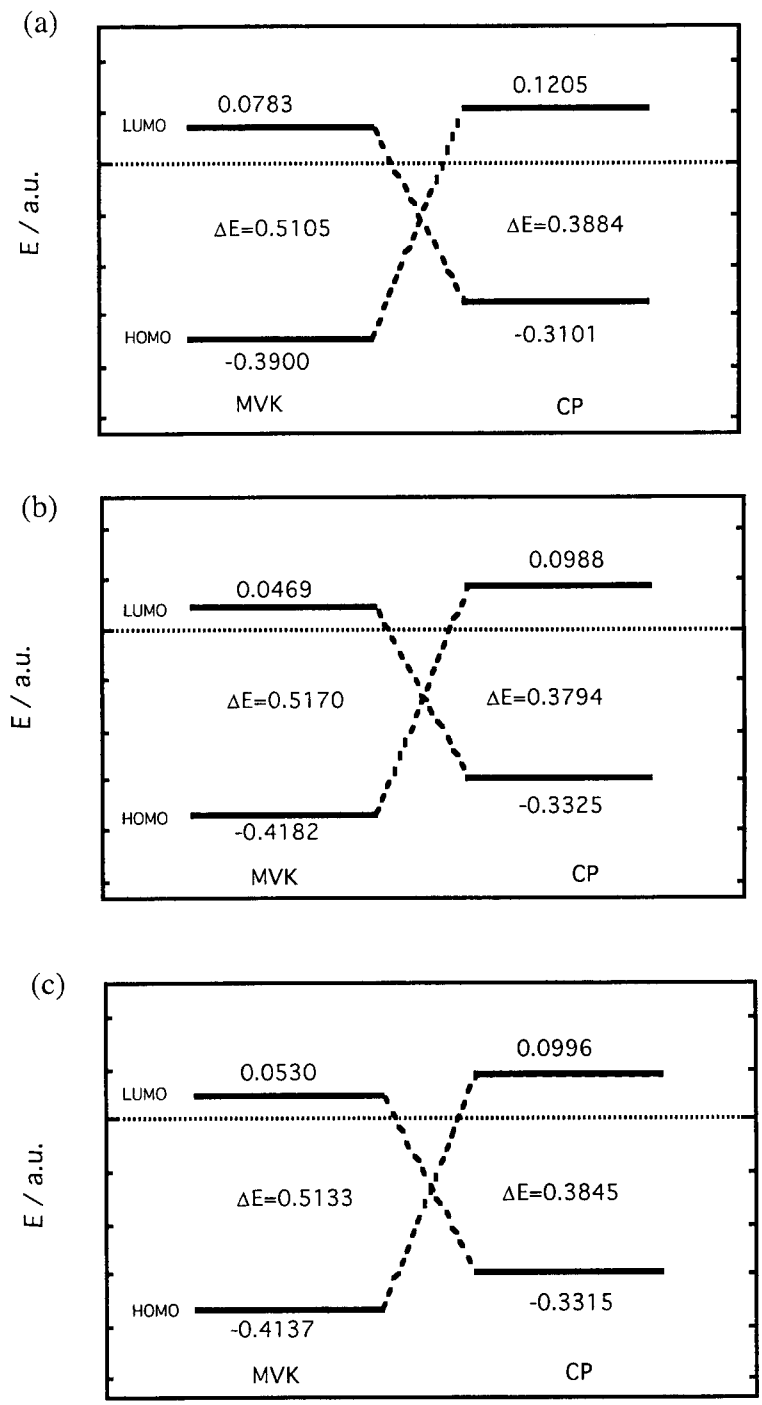

Figure 2.6: HOMO and LUMO energy of CP and MVK in gas phase (a), in AW (b), and in SCW (c).

in between those in gas and in AW. These results seem quite reasonable if one considers that the density of water molecules in SCW is low and that the solvation effect in SCW is less than that in AW. However, substantial effects of solvent to the chemical reactions still remains in SCW.

The computed nodal structure of the LUMO of MVK in aqueous solution is the same with that in gas phase, but the lobe of the electronic wave function around the carbonyl group becomes much greater while that around the π C=C bond becomes smaller (Figure 2.7). In addition to the hydrophobic and hydrogen-bonding effects from solvent, which has been discussed earlier in the section, the enlarging of the lobe at the carbonyl group might be another origin to enhance the selectivity in AW and in SCW compared to that in gas phase, since it increases the secondary orbital interaction. The solvation effect on the orbitals and their energy can be understood in terms of a "substitution effect"; the substitution effect from the carbonyl group in the dienophile is largely enhanced by the hydrogen bonding, which makes the electron-attracting nature of CO group greater, and affects the character of the orbitals.

2.4.2 Solvation Structure

Figure 2.8(a) shows the radial distribution functions (rdf's) of water oxygen and hydrogen around the carbonyl oxygen of MVK, TS, and the product in AW. The height of the first peak in the hydrogen rdf's directly shows degree of hydrogen bonding that causes increase in the dipole moment of the solute molecule. The rdf's for the *endo* reaction indicate that there is no significant change in the solvation structure in the course of the reaction from the reactant to the TS. Since a water molecule cannot access to the carbonyl oxygen of the TS geometrically more than to that of the reactant MVK, the structure of hydration seems to be saturated. However, as mentioned previously, the solvation enhances electronic polarization of the solute molecule in TS, which is manifested in the considerable increase of the $\delta\Delta E_{re}$. The hydrogen bonding is certainly enhanced in the product. The hydrogen bonding which is conspicuous in AW is largely lost in SCW as seen in Figure 2.8(b). The enhanced hydrogen bonding effect cannot be expected in SCW, indicating that the electrostatic effects due to the hydration become relatively small

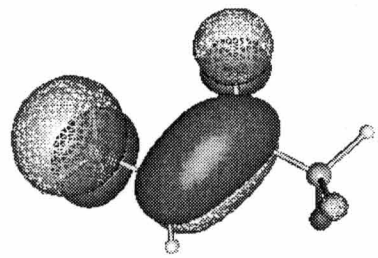

in gas phase

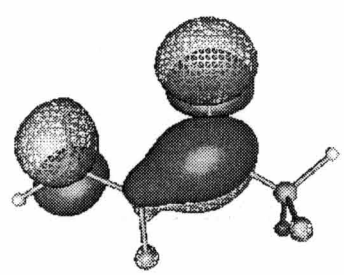

in aqueous solution

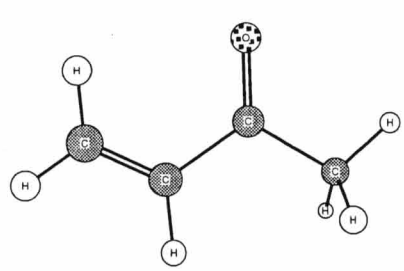

Figure 2.7: LUMO of MVK in the gas phase (top) and in AW (middle).

compared to the hydrophobic effect.

2.4.3 Comparison of the Energetics between Endo and Exo Reactions

In this part, the *endo/exo* selectivity will be discussed from the view point of its dependency on thermodynamic conditions. The stereo-selectivity of the products in AW and in SCW were examined by evaluating the relative equilibrium constant and the relative rate constant. The conditions of the solvent water we employed are as follows: 298.15 K, 1.0 g/cm^3; 373.15 K, 1.0 g/cm^3; 473.15 K, 0.6 g/cm^3; 673.15 K, 0.6 g/cm^3; 873.15 K, 0.6 g/cm^3.

Suppose the yield is determined only by the heat of reactions, then the *endo/exo* ratio is equal to the relative equilibrium constant. In our case, the relative equilibrium constant is determined by the free energy difference between the *endo* and *exo* products. In Table 2.6, the *endo/exo* ratio with respect to the five different conditions are shown. The expression 'δ_r' stands for energies of the *endo* product relative to those of the *exo*. As is listed in the table, the *endo/exo* ratio in AW is the largest among all the conditions examined, but the value itself is relatively small compared to the experimental result for CP-methyl acrylate reaction, 25 : 1 *endo-exo* ratio, in AW.[24] The reaction through the trans TSs have been neglected in this analysis. That might be a reason why we had the small *endo/exo* value. Nevertheless, the theoretical prediction is in qualitative accord with experiment with respect to general trend of solvent effect on the stereo-selectivity.

Among the components of the energy difference bringing out the selectivity, difference in the solvation free energy ($\delta_r \Delta\delta\mu$) mainly contributes to the product stereo-selectivity in AW. As temperature of solvent increases and density decreases, the difference of the solvation free energy becomes less, while the other energy components are changed very little. In the supercritical condition, the difference of the solvation free energy vanishes, and so does the *endo/exo* selectivity. It is predicted that the *endo* and *exo* products in SCW are synthesized at the same ratio when the solvent water reaches the supercritical condition.[4] Although the experimental reaction system is somewhat different from ours, the computational results are in harmony with the experiments.

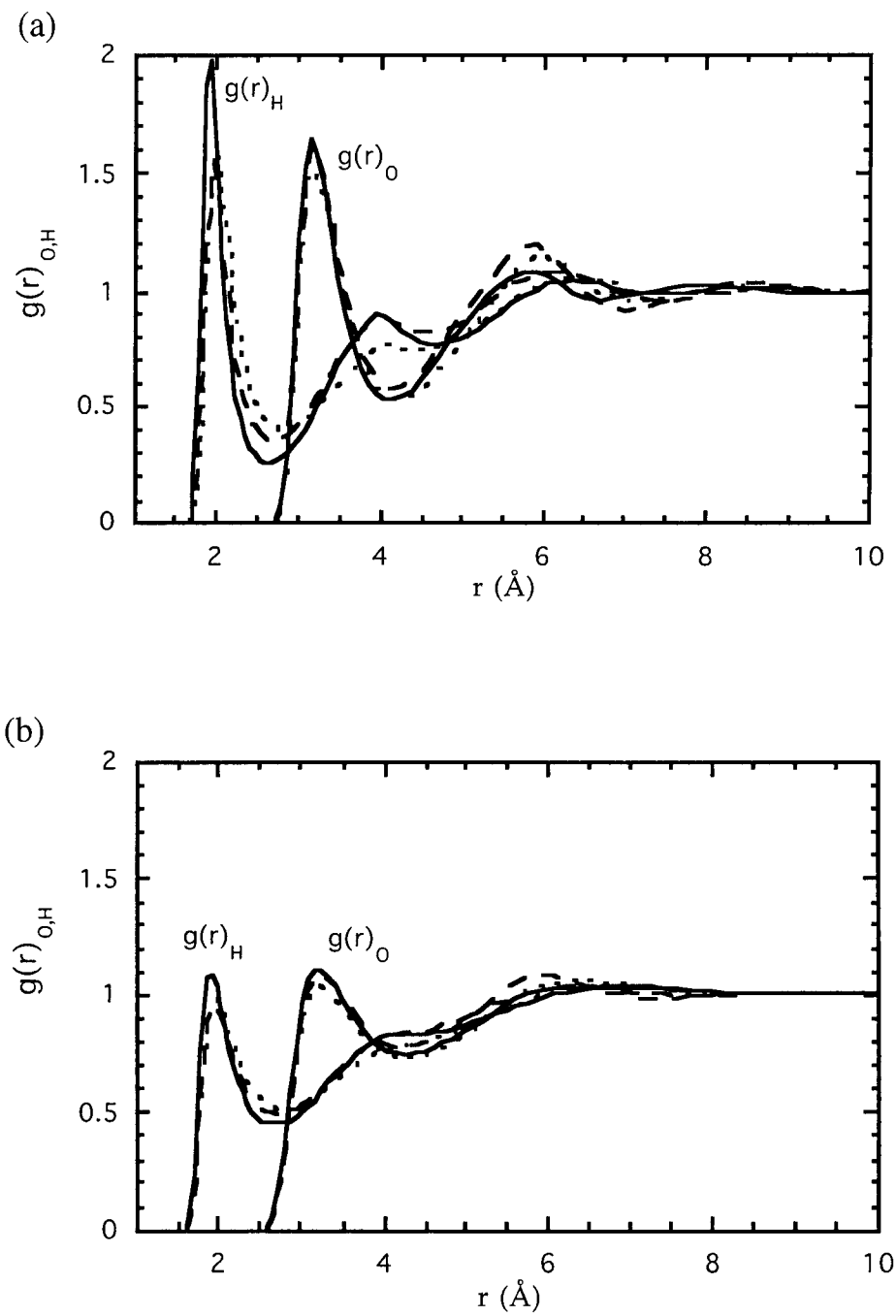

Figure 2.8: Radial distribution functions of water oxygen (g_{O}) and hydrogen (g_{H}) around the carbonyl oxygen of MVK (dashed line), the *endo* TS (dotted line) and the *endo* product (solid line) in AW (a), and in SCW (b).

Table 2.6: Relative energies (kcal/mol) of the *endo* to the *exo* product and the *endo/exo* ratios

temp.[a]	density [b]	$\delta_r\Delta G_{id}^{\phi}$	$\delta_r\Delta E_{solv}^{elec\phi}$	$\delta_r\Delta\delta\mu^{\phi}$	$\delta_r\Delta F_{solv}^{total\phi}$	*endo/exo*
298.15	1.0	-0.29	0.96	-1.84	-1.17	7.20
373.15	1.0	-0.35	0.94	-1.81	-1.22	5.18
473.15	0.6	-0.41	0.80	-1.23	-0.84	2.44
673.15	0.6	-0.53	0.74	-1.07	-0.86	1.90
873.15	0.6	-0.66	0.71	-0.10	-0.05	1.03

In [a]Kelvin and [b]g/cm^3

Figure 2.9 shows the rdf's of the water hydrogen and oxygen around the carbonyl oxygen of the *endo* and *exo* products in AW, indicating height of the first peak is almost the same. This result shows that the both products can make the hydrogen bonding in almost the same strength, and that there is no difference in the hydrogen bonding effects between the two isomers. The *exo* product would expose the nonpolar sites to water solvent more than the *endo* product, and thus hydrophobic effect favors the *endo* product in AW, which is more compact. Therefore, it can be concluded that the large value of the *endo/exo* ratio in AW arises from difference in the hydrophobicity between the *endo* and *exo* products, and that the difference virtually disappears in SCW.

Suppose the rate of the reaction simply follows the Arrhenius equation, then the relative reaction rate can be obtained from the energy difference between the*endo* and *exo* TSs. For the three thermodynamic conditions with 0.6 g/cm^{3}and higher temperatures, difference of the activation free energies ($\delta_r\Delta F_{solv}^{total\ddagger}$) and the relative rate constant (k_{endo}/k_{exo}) are listed in Table 2.7. The RISM-SCF calculations for the *exo* TS were not converged when the solvent conditions are set up at 298.15 K, 1.0 g/cm^{3}and 373.15 K, 1.0 g/cm^3. At the three conditions for which the RISM-SCF results are obtained, $\Delta F_{solv}^{total\ddagger}$ for the *endo* TS is less than that for the *exo* TS, and the value of k_{endo}/k_{exo} seems to decrease with increasing temperature, but the change is very little. The rate preference of the *endo* reaction that depends on the solvent condition seems to be minor.

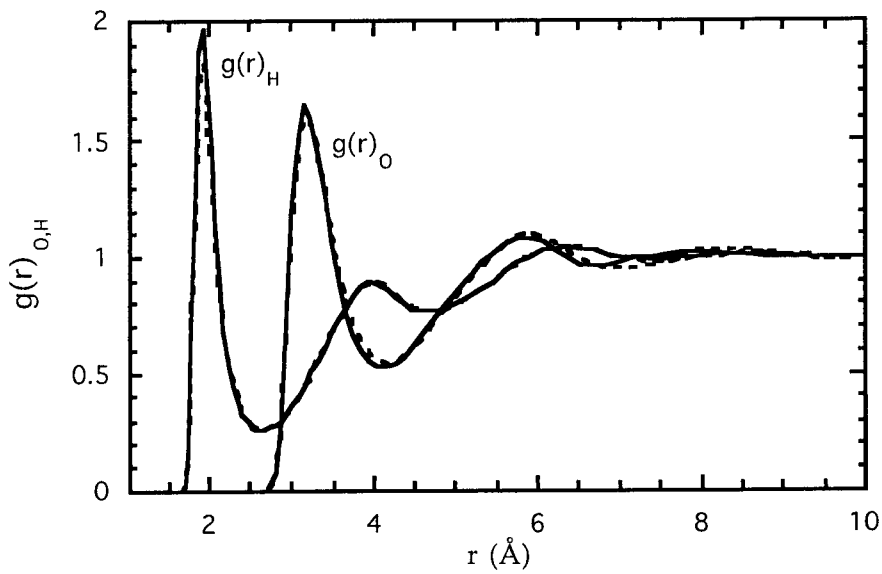

Figure 2.9: Radial distribution functions of water oxygen (g_{O}) and hydrogen (g_{H}) around the carbonyl oxygen of the *endo* product (solid line) and the *exo* product (dashed line)

Table 2.7: Relative activation free energies (kcal/mol) and rate constant of the *endo* to the *exo* TS

temp.[a]	density [b]	$\delta_r\Delta G^{\ddagger}_{id}$	$\delta_r\Delta E^{elec\ddagger}_{solv}$	$\delta_r\Delta\delta\mu^{\ddagger}$	$\delta_r\Delta F^{total\ddagger}_{solv}$	k_{endo}/k_{exo}
298.15	1.0	-0.18	—	—	—	—
373.15	1.0	-0.21	—	—	—	—
473.15	0.6	-0.26	-0.34	0.02	-0.58	1.85
673.15	0.6	-0.34	0.02	-0.41	-0.73	1.73
873.15	0.6	-0.43	0.09	-0.53	-0.87	1.65

In [a]Kelvin and [b]g/cm^3

2.4.4 Conclusion

The stereoselectivity of Diels-Alder reaction in AW and in SCW have been examined, and it was found that the *endo* preference seen in the gas phase is more pronounced in AW. For the activation free energy in AW, the hydrophobic effect, which stabilizes the transition states, is undoubtedly an important factor. The enhanced hydrogen bonding does also play an important role for decreasing the activation free energy. At the same time, however, it increases the electronic energy of the transition state. The increase of the electronic energy sometimes compensate largely the decrease of the solvation free energy. The free energy change for the reaction is decreased by both hydrophobic and hydrogen bonding effects. In SCW, solvent effects characteristic to water become weaker, and degree of the stabilization is less.

Regarding the *endo/exo* selectivity in this system, the hydrophobic effect is the main contribution in AW: the more compact product which is favored with respect to the hydrophobic effects is synthesized preferentially. In SCW, difference in the hydrophobicity for the products disappears, and dose the *endo/exo* selectivity. Considering the energetics of the TSs, the *endo* reaction occurs preferentially, and the *endo/exo* relative rate is expected to be constant in the wide range of solvent conditions, though it is not conclusive at the moment since the RISM-SCF calculation was not converged. The TS and the product seem to have similar geometry, but the slight difference in geometry produces the difference of the solvation free energy, and their energetics would never be the same due to the electronic structure change coupling with solvent water.

The frontier orbitals of the reactant were greatly polarized by the solvent effects compared to those in the gas phase. In the present reaction system, substitution effect from the carbonyl group in the dienophile is largely enhanced by the hydrogen bonding, which makes the electron-attracting nature of CO group greater, and affects the character of the orbitals as well as the reaction energetics.

Bibliography

[1] Rideout, D.; Breslow, R. *J. Am. Chem. Soc.* **1980**, *102*, 7816.

[2] Shaw, R. W.; Brill, T. B.; Clifford, A. A.; Eckert, C. A.; Franck, E. U. *Chem. Eng News 26,*1991, Dec. 23.

[3] Savage, P. E. *Chem.. Rev.*, **1999**, *99*, 603.

[4] Korzenski, M. B.; Kolis, J. W. *Tetrahedron.Lett.* **1997**, *38*, 5611.

[5] Luo, H.; Tucker, S. C. *J. Am. Chem. Soc.* **1995**, *117*, 11359.

[6] Luo, H.; Tucker, S. C. *J. Phys. Chem.* **1996**, *100*, 11165.

[7] Luo, H.; Tucker, S. C. *J. Phys. Chem. B* **1997**, *101*, 1063.

[8] Pomelli, C. S.; Tomasi, J. *J. Phys. Chem. A* **1997**, *101*, 3561. Bennet, G. E.; Rossky, P. J.; Johnston, K. P. *J. Phys. Chem.* **1995**, *99*, 16136.

[9] Balbuena, P. B.; Johnston, K. P.; Rossky, P. J. *J. Am. Chem. Soc.* **1994**, *116*, 2689.

[10] Balbuena, P. B.; Johnston, K. P.; Rossky, P. J. *J. Phys. Chem.* **1995**, *99*, 1554.

[11] Flanagin, L. W.; Balbuena, P. B.; Johnston, K. P.; Rossky, P. J. *J. Phys. Chem.* **1995**, *99*, 5196.

[12] Ten-no, S.; Hirata, F.; Kato, S. *Chem. Phys. Lett.*, **1993**, *214*, 391.

[13] Ten-no, S.; Hirata, F.; Kato, S. *J. Chem. Phys.*, **1994**, *100*, 7443.

[14] Sato, H.; Hirata, F.; Kato, S. *J. Chem. Phys.*, **1996**, *105*, 1546.

[15] Sato, H.; Hirata, F. *J. Phys. Chem. B* **1999**, *103*, 6596

[16] Blake, J. F.; Jorgensen, W. L. *J. Am. Chem. Soc.* **1991**, *113*, 7430.

[17] Blake, J. F.; Lim, D.; Jorgensen, W. L. *J.Org.Chem.* **1994**, *59*, 803.

[18] Otto, S.; Blokzijl, W.; Engberts, Jan B. F. N. *J.Org.Chem.* **1994**, *59*, 5372.

[19] Furlani, T. R.; Gao, J. *J.Org.Chem.* **1996**, *61*, 5492.

[20] Jorgensen, W. L.; Lim.D.; Blake, J. F. *J. Am. Chem. Soc.* **1993**, *115*, 2936.

[21] Jorgensen, W. L.; Madura, J. D.; Swenson, C. J. *J. Am. Chem. Soc.* **1984**, *106*, 6638.

[22] Jorgensen, W. L.; Briggs, J. M.; Contreras, M. L. *J. Phys. Chem.* **1990**, *94*, 1683.

[23] Assfeld, X.; Ruiz-Lopez, M. F.; Garcia, J. I.; Mayoral, J. A.; Salvatella, L. J. *J. Chem. Soc.Commun*, **1995**, 1371.

[24] Breslow, R.; Maitra, U. *Tetrahedron.Lett.* **1984**, *25*, 1239.

[25] Huzinaga, S. *J. Chem. Phys.* **1965**, *42*, 1293.

Freisner, R. A. *J. Phys. Chem.* **1998**, *92*, 3091

[26] Berendsen, H. J. C.; Postma, J. P. M.; van Gunstern, W. F.; Hermans, J. In *Inter molecular Forces*; Pullmann, B., Ed.; Reidel: Dordrecht,1981.

[27] Singer, S. J.; Chandler, D. *Mol. Phys.*, **1985**, *55*, 621.

[28] Pierotti, R. A. *Chem. Rev.*, **1976**, *76*, 717.

[29] Ortuño, R. M.; Ballesteros, M.; Corbera, J.; Sanchez-Ferrando, F. *Tetrahedron*, **1988**, *44*, 1711.

[30] Fukui K.; Yonezawa, T.; Shingu, H. *J. Chem. Phys.* **1952**, *20*, 722. : Fukui, K. *Acc. Chem. Res*, **1971**, *4*, 57.

[31] Woodward, R. B.; Hoffmann, R. *J. Am. Chem. Soc.* **1965**, *87*, 395. :Woodward, R. B.; Hoffmann, R. "*The Conservation of Orbital Symmetry*", Academic Press, New York, 1969.

[32] Chandler, D.; Andersen, H.C. *J. Chem. Phys.* **1972**, *57*, 1930.

[33] Hirata, F.; Rossky, P.J. *Chem. Phys. Lett.* **1981**, *83*, 329. Singer, S. J.; Chandler, D. *Mol. Phys.*, **1985**, *55*, 621.

Chapter 3

Partial Molar Volume of Biomolecules

3.1 Introduction

Revealing the phenomena of life is one of the most challenging work in modern science. In the late 1940's and 1950's, the revolution in modern molecular biology began. The direct connection of "one gene-one enzyme" was established. The basic structure of double-strand DNA was proposed. Some inspired guessing provided the rationale for the Central Dogma: DNA $\rightarrow$ RNA $\rightarrow$ protein.[1)] Basically, DNA and RNA only have a genetic information, whereas proteins show great diversity in physical properties, ranging from water-soluble enzymes to the insoluble keratine of hair and born, and they perform a wide range of biological functions. Therefore, studying proteins is one of the most important key for revealing the phenomena of life.

It has long been known that dramatic changes occur in the properties of protein upon heating or acidification. Although the end result was frequently visible coagulation, an essential first step in the process was called *denaturation.* It was shown in the early 1930's that some of these early changes can be reversed with recovery of biological function, and this process was called *renaturation.* The probable nature of these reactions as conformational change involving expanding or contracting a polymer chain was also pointed out at that time. However, there was not uniform agreement on the *denaturation/renaturation* reaction.[2)]

In 1952, it was proven that the basic covalent structure of a protein is a linear peptide chain and that amino acid sequence of the chain is unique for a given protein. Just after that, the fundamental significance of the *denaturation/renaturation* reaction became clear through the pioneering studies of Anfinsen. By showing that a unfolded polypeptide chain could spontaneously refold to form a native protein with full biological activity, (The *denaturation/renaturation* reactions are most commonly referred to as *unfolding and folding*, though, strictly speaking, they are not the same.) Anfinsen concluded that this sequence, by itself, contains all of the information necessary to define the three-dimensional structure of the protein and, thus, its biological function.[3] Only the composition and properties of the solvent have to be adjusted for the reaction to occur and for biological function to appear in the folded product. There is no requirement for mysterious biological "factors". Then, the problem presented by the folding reaction has become perhaps the clearest and most general example of the complex interface between chemistry and biology.

3.1.1 Protein Structure

Proteins are naturally with molecular weight greater than 5,000. These *macromolecules* show great diversity in physical properties found in a living thing, and they perform a wide range of biological functions. With the resolution at an atomic level, their structures are quite huge and complex, and each of proteins has a unique structure of itself. However, it has been found that they share a common molecular structure as follows.

Primary Structure

There are 20 different amino acids used in the synthesis of proteins; these amino acids, which have just 20 different side chains, are listed in Figure 3.1.[4,5] As a matter of course, these amino acids influence the physical properties of proteins. The side chains of the nonpolar or the aromatic or the aliphatic (hydrophobic) group play an important role in stabilizing protein in aqueous solution as an hydrophobic interaction.[6] The side chains of the polar or the charged (hydrophilic) group are also important in having an electrostatic interaction, which is effective within a protein molecule or between a protein and solvent molecules. The property of the charged (dissociative) group can be changed by pH con-

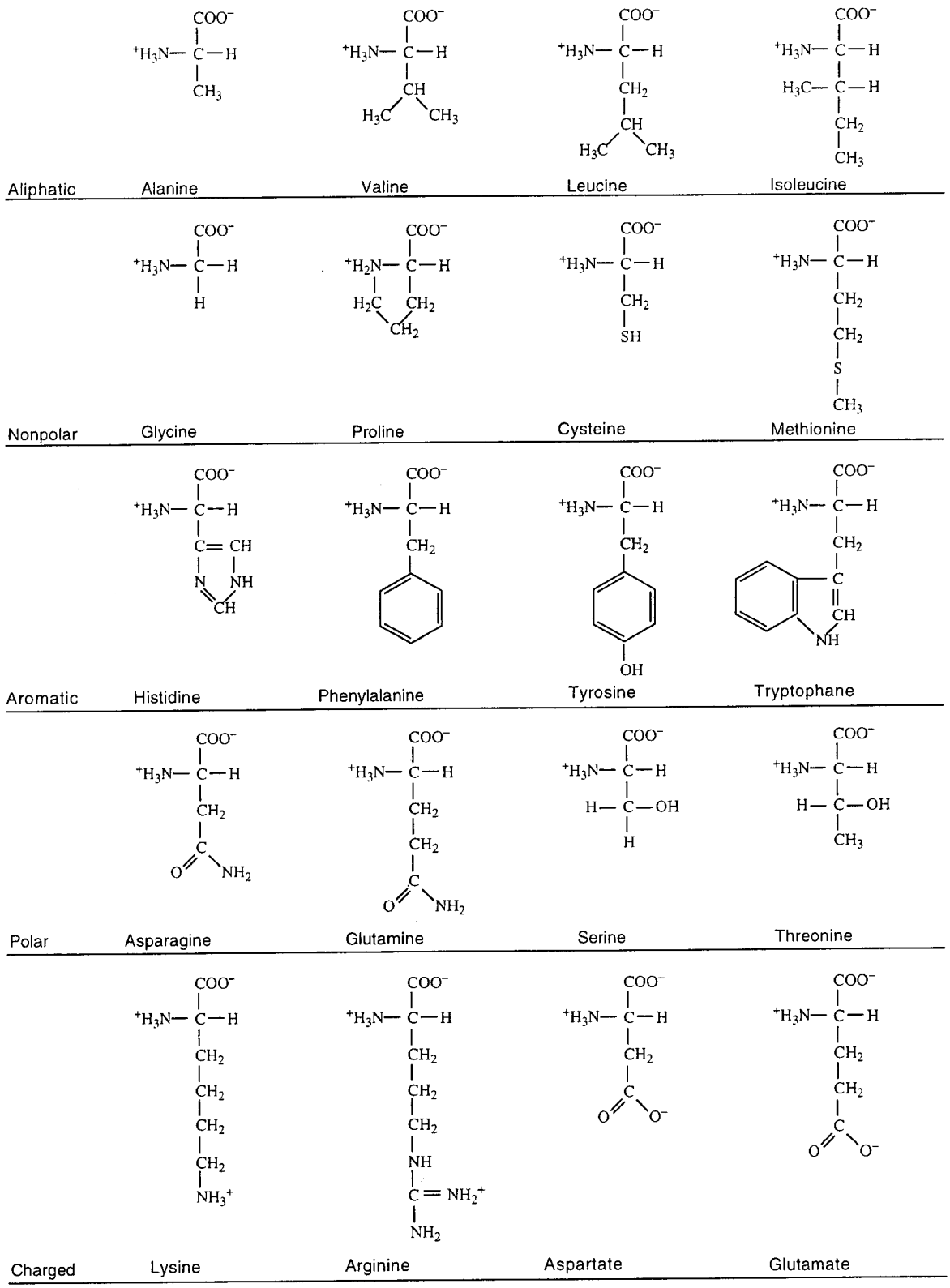

Figure 3.1: Structures of amino acids naturally found in proteins

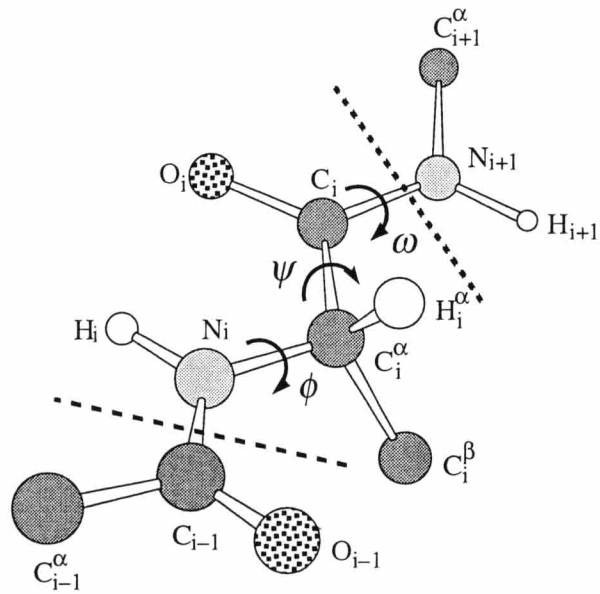

Figure 3.2: The definition of dihedral angle of a polypeptide main chain

dition of solvent, and consequently its contribution in a protein stability is altered. The linear sequence by peptide bonds between the 20 amino acids with its own individuality is usually defined as "primary structure".

Secondary Structure

The regular, repeating folding pattern (such as the α helix and β structures), stabilized mostly by hydrogen bond between peptide groups close together in the sequence, are called "secondary structure". Figure 3.2 shows the dihedral angle of a polypeptide main chain. In this structure, the amino-acid unit is divided by the dashed lines. Because the peptide group itself is rigid and planer, there is no rotation around the bond between the carbonyl carbon atom and the nitrogen atom (the $C_i - N_{i+1}$ bond). However, free rotation is possible around the bond between the α carbon and the carbonyl carbon atom (the $C^{\alpha}_i - C_i$ bond) and about the bond between the nitrogen atom and the α carbon (the $C^{\alpha}_i - N_i$ bond). Thus, for every peptide group in a protein, there are two rotatable bond (Φ and Ψ) the relative angles of which define a particular backbone conformation.

In the α helix, polypeptide backbone is folded in such a way that the carboxyl group of each amino acid residue is hydrogen-bonded to the amino group of the fourth residue

along the chain. The backbone of the α helix winds around the long axis, as shown in Figure 3.3(a). The hydrogen bonds are all aligned approximately parallel to this axis, and the side chain protrude outward. Each residue is spaced 0.15 nm from the next along the axis, and 3.6 residues are required to make a complete turn of the helix. The right-handed α helix usually has Φ and Ψ values of -57° and -47°, respectively. Because each carboxyl and amino group is hydrogen-bonded (except the four at each end), the α helix is strongly stabilized. However, for some amino acids (e.g., glycine, proline) interactions involving the side chains may weaken the α helix, making this conformation less likely in polypeptide chains containing high proportions of such helix-destabilizing amino acids.

The second major regular, repeating structure, the β structure, differs from the α helix in that the polypeptide chains are almost completely extended, as in Figure 3.3(b). The hydrogen bonding occurs between polypeptide strands, rather than within the single strand. Adjacent chains can be aligned in the same direction as in the *parallel* β sheets, or alternate chain may be aligned in opposite orientations as in the *antiparallel* β sheets. These structures often form extensive sheets. Sometimes it is possible for several sheets to be stacked upon one another. Because the side chain tend to protrude above and below the sheet in the alternating sequence, the β-sheet structures are favored by amino acids with relatively small side chains, such as alanine and glycine. Large, bulky side chains can lead to steric interference between the various parts of the protein chain.

Tertiary Structure

For a globular protein, tertiary structure means the way that segments of the secondary structure fold together in three dimensions, stabilized by interactions often far apart in the sequence. For those proteins with little or no detectable α helix and β structure, the tertiary structure can be considered the way the protein folds in three dimensions, stabilized by interactions between distant parts of the sequence. Since the structural analysis of myoglobin by x-ray crystallography, many protein and enzymes have been examined, and in many way, a clear secondary-tertiary structure distinction cannot be so easily made. However, some generalizations can be made from these studies. Most electrically charged groups are on the surface of the molecule, interacting with water.

(a) α-helix

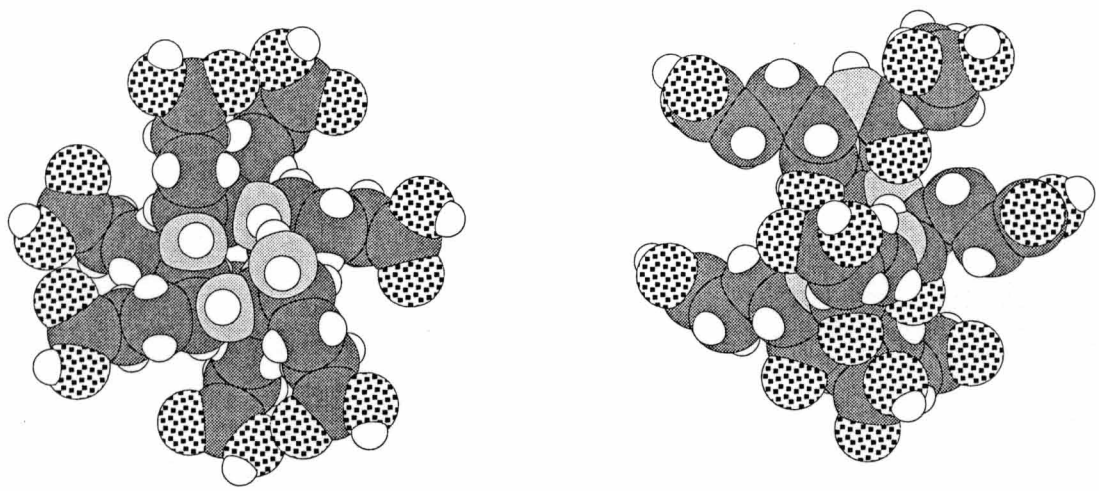

(top view) (side view)

(b) extended

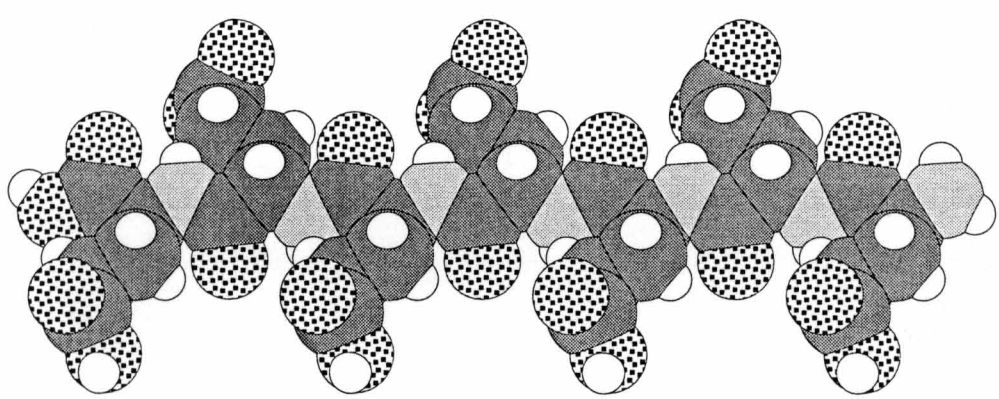

Figure 3.3: The molecular model of glutamate heptamer in the α-helix (a) and the extended form (b). The dark-gray, light-gray, and white balls indicate carbon, nitrogen, and hydrogen atoms, respectively. The balls with dots mean oxygen atoms.

Exception to this rule are often catalytically important residues in enzyme, which are often partially stabilized by specific polar interactions within a hydrophobic portion of the molecules. Most nonpolar groups are in the interior of the molecule, avoiding the thermodynamically unfavorable contact with water. Exception to this may function as specific binding sites on the molecule for other protein ligands.

3.1.2 Protein Denaturation and Thermodynamics

The structures of proteins can be stable in solution under the physiological conditions; room temperature, normal pressure, and neutral pH. When these conditions are extremely changed, however, the protein structure is broken without breaking its covalent bonds. This phenomenon is called the "denaturation". The expression originally means that proteins lose their biological functions. But it is most commonly now referred to as "unfolding" of the protein structures. The protein denaturation or unfolding process is thus regarded as the transition from the ordered (N) state where the three-dimensional structure is defined at Ångström level to more disordered (D) state. Accompanying this process, the biological functions of proteins are usually lost. It should be noted that the process we are concerned with is essentially reversible.

Both the N state and the D state are actually the ensemble of the huge number of microscopic states, and thus, called the thermodynamic states. Here, the microscopic states should define the coordinates and momenta of the atoms composing a protein molecule. Provided that the two thermodynamic states does not include the same microscopic states each other, the difference of the Gibbs free energy between the N state and the D state determines which state a protein molecule should be in. Then, the elementary form of the folding reaction is simple:

$$\begin{array}{ccc} N & \xrightarrow{unfolding} & D \\ folded & \xleftarrow[folding]{} & unfolded \end{array}$$

For an elementary equilibrium process such above, the following general expression holds:

$$\Delta_N^D G = p\Delta_N^D V - T\Delta_N^D S, \tag{3.1}$$

where $\Delta_N^D G$, $\Delta_N^D V$, and $\Delta_N^D S$ are the changes in Gibbs free energy, volume, and entropy, accompanied with the denaturation; p is the pressure, T the temperature. The physical

variable p and T may change the sign of $\Delta_N^D G$. It should be noted that the situation would become more complex when the two thermodynamic state include the same microscopic states. The Gibbs energy of the N state is lower than that of the D state by at most 40 kJ/mol at room temperature. As a matter of course, the difference between them are diminished at the temperature of the thermal transition. The temperature dependence of the difference is approximated to be -1.5 kJ/K·mol. Considering the thermal energy is about 2 kJ/mol, the N state and D state are coexisted within a range of 10K around the temperature of the thermal transition. The temperature range of the transition is relatively wide in comparison with the solid-liquid phase transition.

The temperature dependence of the Gibbs free energy change can be expressed:

$$\Delta_N^D S = -\left(\frac{\partial \Delta_N^D G}{\partial T}\right)_p, \tag{3.2}$$

and the heat capacity change accompanied with the thermal denaturation, $\Delta_N^D C_p$, are also obtained as

$$\left(\frac{\partial^2 \Delta_N^D G}{\partial T^2}\right)_p = \frac{\Delta_N^D C_p}{T}. \tag{3.3}$$

The value of the heat capacity change, which is the second derivative of the Gibbs free energy change, is found to be negative, thus the Gibbs free energy change as a function of temperature is convex. This result implies the denaturation would occur in low temperature-side as well as high temperature-side, where the Gibbs free energy change becomes zero. This phenomenon is confirmed by experiments and called "cold denaturation".[7] The cold denaturation is recognized to be general nature of proteins, which have the negative $\Delta_N^D C_p$.

For the pressure-induced transition, the $\Delta_N^D V$ plays the same part as the entropy change does in the thermal transition, and expressed as

$$\Delta_N^D V_T = \left(\frac{\partial \Delta G_N^D}{\partial p}\right)_T. \tag{3.4}$$

At a constant temperature, the pressure induces the volume decreasing, accompanied with the protein denaturation. The second derivative of the Gibbs free energy with pressure is given by the expression:

$$\left(\frac{\partial^2 \Delta_N^D G}{\partial T^2}\right)_T = -V\left(-\frac{1}{V}\frac{\partial^2 \Delta_N^D V}{\partial T^2}\right)_T = -V\beta_T, \tag{3.5}$$

where β_T is isothermal compressibility. The protein denaturation usually occurs under high pressure over 3000 atm.[8,9] It is obvious that the volume of the system decrease accompanied with that. Moreover, it is pointed out that the isothermal compressibility increases with the protein denaturation by employing high pressure. Consequently, the carveture of the Gibbs free energy change is also negative as a function of pressure. With the same logic as thermal denaturation, there exist the pressure where proteins are most stable, and the protein denaturation may occur in both high and low pressure regions as well as temperature. Recently, much interest has been focused on the pressure effect of protein, and high-pressure studies are active. It should be noted that the thermodynamic properties of the denaturation discussed above supposes the two state transition between the N and D states; i.e., the heat denatured state and the cold denatured state are the same thermodynamic state. However, there is no guarantee that every protein is denatured with the two-state like manner, for it has been reported that intermediate states; so called "molten globule" are found to have a thermal transition,[10] and that the heat absorption is detected in the change from the cold-denatuared state and the heat-denatuared state for a certain protein,[11]

The most significant difference between the N state and the D state is in that the atoms buried inside the protein are expose to solvent water molecules. Therefore, the interactions between atoms of the N state are different from that of the D state. In order to obtain molecular aspect of protein from the thermodynamic properties, the solvent molecules must be included for the system. For the heat-denaturation, random structures may be favored in high temperature because of increase in the entropy of the polypeptide chain. However, this interpretation will be obviously invalid for the cold-denaturation. Then, the solvation effect for the thermodynamic properties must be included for more accurate interpretation. For the pressure-induced denaturation, although the N states might be intuitively regarded as the most compact structure, the D state should be the most compact structure. This would be able to be explained by including the solvation structure of both states.

3.1.3 High Pressure Effects on Protein Structure

Since Bridgeman's pioneering work in 1914,[12] showing that a pressure of 7 kbar is able to denature proteins of egg white in a similar but not identical way as temperature, pressure has been long disregarded by biochemists. The reason was the absence of general ideas on what can be added by studying the pressure effects to understand the behavior of proteins. In addition, the lack of basic concepts about pressure effects on biochemical reactions and structure of biopolymers did not stimulate activities in this field.

In recent decades, however, there has been a growing interest by the researchers introducing pressure as a variable acting on biosystems.[13,14] One of the reasons is the possibility of applying pressure in specific biotechnological area. It has also become clear that pressure can be used for more detailed thermodynamic and kinetic description of biosystems. As mentioned in the previous section, along with such parameter as temperature and solvent conditions, pressure is essential for the ultimate understanding of protein denaturations.[15,16] Due to technical progress in the last decade, many instrumental problems that hampered high-pressure research have been solved.

Pressure effects are governed by Le Chatelier's principle, which states that at equilibrium a system tends to minimize the effect of any external perturbation. Consequently, an increase in pressure favors reduction of the volume of the system. The volume change, which is the difference between the volumes of the final (V_f) and initial (V_i) state, is given by the expression:

$$\Delta_i^f V = V_f - V_i = \left(\frac{\partial \Delta_i^f G}{\partial p}\right)_T = -RT\left(\frac{\partial \ln K}{\partial p}\right)_T, \tag{3.6}$$

where K is the equilibrium constant governing the process. In case of the protein denaturation, the initial and the final state can be exchanged by the native and the denatured state. It should be noted that the "volume" must be the partial molar quantity when chemical equilibrium is concerned. Therefore, the partial molar volume (PMV) is the thermodynamic quantity that plays an essential role in the analysis of pressure effects on protein denaturation as well as chemical reactions and chemical equilibrium in solution.

Experimental and Theoretical Study for Partial Molar Volume

A considerable amount of experimental work has been devoted to measure the PMV of a variety of solute in many different solvents, and has contributed to extract information of molecular interactions in solution.[17,18] However, analysis and interpretation of the experimental data have been in many cases based on drastically-simplified models of solution or on speculations without physical ground, even for the simplest solute such as alkali-halide ions in aqueous solutions. Difficulty of molecular interpretation of the quantity increases dramatically when it comes to biomolecules such as protein, because those molecules feature complicated geometry as well as interactions with solvent molecules. Maneuvers commonly employed in analysis of experimental data are to decompose the volume into several contributions more or less intuitively, and express the entire volume by a superposition of those contributions. For example, substantial effort is devoted to decompose the PMV of amino acids into contributions from constituent atomic groups.[18-20] Obvious difficulty faced by those empirical decomposition is that the volume assigned to an atom group is very much dependent on the environment where the group is located. Even more difficult is consideration of conformational fluctuations characteristic to those molecules.

Unlike experimental efforts, theoretical studies of a PMV are very limited.[21-27] Although molecular simulations for the PMV have been started a few years ago,[28,29] computational time limitations still constitute an obstacle for their application to such a large system as a protein molecule. On the other hand, there are only a few studies based on the statistical mechanics of liquids.[30] The scaled particle theory was applied to calculate the PMV of a spherical ion in aqueous solution from the free energy of cavity formation in liquid.[21] Although it successfully provided a microscopic picture for an "intrinsic volume" which is defined as the volume of a hypothetical ion without charge,[17] it has an inherent weakness in that the molecular interactions cannot be treated explicitly.

Another method is based on the Kirkwood-Buff (KB) theory[33] which provides a general framework for evaluating the thermodynamics, including the PMV of a liquid mixture in terms of the pair density correlation functions. Recently, Imai, Kinoshita, and Hirata[34] derived the KB equation for molecular solutions based on the reference interaction site

model (RISM) integral equation theory,[35-40] and applied the method to calculate the PMV of amino acids. The theory was found to be successful in the sense that it can take account for chemical specificities of amino acids manifested in their PMV. The results, however, showed a systematic negative deviation from the corresponding experimental data, which increases nearly proportionally to the number of atoms in the amino acid. From the temperature dependence of the PMV, the deviation has been attributed to the "ideal fluctuation volume" which accounts for the ideal gas contribution originating from non-rigidity of a molecule. However, even with the ideal contribution added, there still exists a systematic deviation, not explained yet. Moreover, a straight application of the KB-RISM method to the PMV change in a conformational transition of a polypeptide produces results contradictory to experiment. All these indicates that the conventional, one-dimensional (1D) RISM procedure essentially underestimates volume exclusion effects, especially for molecules comprising a large number of atoms.

The three-dimensional (3D) RISM method,[41-45] which accounts for the excluded volume effects much better than the conventional RISM approach, is expected to be valid to evaluate the PMV of macromolecules such as biomolecules. In this chapter, the KB and the 3D-RISM theories were coupled to calculate the PMV of 20 amino acids, and also applied to study the PMV change in the helix-coil transition of an oligopeptide of glutamic acids, for which experimental data are available.

3.2 Methods

3.2.1 Three-dimensional RISM Theory

As mentioned in Chapter 1, the description of a molecular liquid is complicated since the interactive potential between polyatomic particles depends on their orientations as well as separations. Actually, the distribution function satisfying the Ornstein-Zernike (OZ) integral equation (1.23) become six-dimensional (6D). For a solute immersed in a molecular solvent at infinite dilution, the OZ equation holds the following expression.

$$h^{UV}(r_{12}, \Omega_1, \Omega_2) = c^{UV}(r_{12}, \Omega_1, \Omega_2)$$

$$+\rho^V \int d\mathbf{r}_3 d\Omega_3 c^{UV}(r_{13}, \Omega_1, \Omega_2)$$
$$\times h_{UV}(r_{32}, \Omega_3, \Omega_2), \tag{3.7}$$

and for pure solvent,

$$\begin{aligned} h^{VV}(r_{12}, \Omega_1, \Omega_2) &= c^{VV}(r_{12}, \Omega_1, \Omega_2) \\ &+\rho^V \int d\mathbf{r}_3 d\Omega_3 c^{VV}(r_{13}, \Omega_1, \Omega_2) \\ &\times h_{VV}(r_{32}, \Omega_3, \Omega_2), \end{aligned} \tag{3.8}$$

where h and c are, respectively, the total correlation functions and the direct correlation functions (DCF's) dependent on the separation between the "origins" of the particles, $r_{21} = |\mathbf{r}_2 - \mathbf{r}_1|$, and on their orientations, Ω_1 and Ω_2, with respect to vector $\mathbf{r}_{12}$. The notations U and V mean solute and solvent, respectively, and ρ^V is the number density of solvent. Recently, a modified approach has been proposed, in which the correlation functions in the initial 6D OZ equation are being averaged over the orientation of only one particle.[41, 49-51)]

In the standard, 1D-RISM theory, the correlation functions h and c are averaged over the orientations of liquid particles at a fixed site separation $r_{\alpha\gamma}$,

$$\Phi^{VV}_{\alpha\gamma}(r_{\alpha\gamma}) = \int d\Omega_1 d\Omega_2 \Phi^{VV}(|\mathbf{r}_{12} - \mathbf{r}_{2\gamma} - \mathbf{r}_{1\alpha}|, \Omega_1, \Omega_2) \tag{3.9}$$

where Φ stands for h or c, and $\mathbf{r}_{i\alpha}$ is the vector between the "origin" of the ith particle and its site α. Their Fourier transforms can be written as

$$\begin{aligned} \Phi^{VV}_{\alpha\gamma}(k) &= \int d\mathbf{r}_{12} \Phi^{VV}_{\alpha\gamma}(r_{\alpha\gamma}) e^{i\mathbf{k}\cdot\mathbf{r}_{12}} \\ &= \int d\Omega_1 d\Omega_2 \Phi^{VV}(k, \Omega_1, \Omega_2) e^{-i\mathbf{k}\cdot\mathbf{r}_{1\alpha} + i\mathbf{k}\cdot\mathbf{r}_{2\gamma}} \end{aligned} \tag{3.10}$$

In the 3D-RISM approach,[43-45)] the 3D correlation functions of solvent sites around the solute that are *partially* averaged over the orientation of solvent molecules,

$$\Phi^{UV}_{\gamma}(\mathbf{r}_{1\gamma}) \equiv \Phi^{UV}_{\gamma}(r_{1\gamma}, \Omega_1) = \int d\Omega_2 \Phi^{UV}(|\mathbf{r}_{1\gamma} - \mathbf{r}_{2\gamma}|, \Omega_1, \Omega_2), \tag{3.11}$$

where $\mathbf{r}_{1\gamma} = \mathbf{r}_\gamma + \mathbf{r}_1$ is the vector from the solute to solvent site γ. Below the coordinate origin is fixed at the solute, $\mathbf{r}_1 = 0$. The corresponding 3D Fourier transforms of the site

correlation functions are

$$\begin{aligned} \Phi_\gamma^{UV}(\mathbf{k}) &= \int d\mathbf{r}_2 \Phi_\gamma^{UV}(\mathbf{r}_\gamma) e^{i\mathbf{k}\cdot\mathbf{r}_2} \\ &= \int d\Omega_2 \Phi^{VV}(k, \Omega_1, \Omega_2) e^{i\mathbf{k}\cdot\mathbf{r}_{2\gamma}}. \end{aligned} \tag{3.12}$$

Much as in the 1D-RISM, the interaction potential between the solute and solvent particles is assumed to be additive,

$$u^{UV}(\mathbf{r}_2, \Omega_2) \equiv u^{UV}(r_{12}, \Omega_1, \Omega_2) = \sum_\gamma u_\gamma^{UV}(\mathbf{r}_\gamma). \tag{3.13}$$

Furthermore, since the long-range asymptotics of the DCF is equal to the interaction potential, $c^{UV}(\mathbf{r}_2, \Omega_2) \sim -\beta u^{UV}(\mathbf{r}_2, \Omega_2)$ for $|\mathbf{r}_2| \to \infty$, the solute-solvent DCF's are broken up into the partial site contributions,

$$c^{UV}(\mathbf{r}_2, \Omega_2) \equiv c^{UV}(r_{12}, \Omega_1, \Omega_2) = \sum_\gamma \tilde{c}_\gamma^{UV}(\mathbf{r}_\gamma). \tag{3.14}$$

This is the basic assumption of the 3D-RISM theory. In reciprocal space, it has the form

$$\begin{aligned} c^{UV}(\mathbf{k}, \Omega_2) &= \int d\mathbf{r}_2 c_\gamma^{UV}(\mathbf{r}_\gamma) e^{i\mathbf{k}\cdot\mathbf{r}_2} \\ &= \sum_\gamma \tilde{c}_\gamma^{UV}(\mathbf{k}) e^{-i\mathbf{k}\cdot\mathbf{r}_{2\gamma}}. \end{aligned} \tag{3.15}$$

Notice the distinction between the *partial* site $\tilde{c}$ and the orientationally averaged site c. The latter is expressed in terms of the former by substituting the decomposition (3.15) into Eq.(3.12),

$$c^{UV}(\mathbf{k}) = \sum_\alpha \tilde{c}^{UV}(\mathbf{k}) \int d\Omega_2 e^{i\mathbf{k}\cdot(\mathbf{r}_{2\gamma} - \mathbf{r}_{2\alpha})}. \tag{3.16}$$

The orientational dependence is thus factored out from the partial site DCF's, $\tilde{c}$. In the familiar form, this is written as

$$c^{UV}(\mathbf{k}) = \sum_\alpha \tilde{c}^{UV}(\mathbf{k}) \omega_{\alpha\gamma}(k), \tag{3.17}$$

where $\omega_{\alpha\gamma}(k) = \sin(kr_{\alpha\gamma})/(kr_{\alpha\gamma})$ is the Fourier transform of the intramolecular pair correlation function, and $r_{\gamma\alpha} = |\mathbf{r}_{2\gamma} - \mathbf{r}_{2\alpha}|$ is the separation of sites in a single molecule.

The 6D solute-solvent OZ equation (3.7) is transformed to reciprocal space and averaged over orientation Ω_2, performing reduction from the orientationally dependent 6D

correlation functions to the 3D site correlation profiles. On substituting the decomposition (3.15), the OZ equation takes the form

$$\begin{aligned} h_\gamma^{UV}(\mathbf{k}) &= \sum_\alpha \tilde{c}_\alpha^{UV}(\mathbf{k})\omega_{\alpha\gamma}(k) \\ &\quad +\rho^V \sum_\alpha d\Omega_3\Omega_2\tilde{c}_\alpha^{UV}(\mathbf{k})e^{-i\mathbf{k}\cdot\mathbf{r}_{3\alpha}} \\ &\quad \times h^{VV}(k,\Omega_3,\Omega_2)e^{-i\mathbf{k}\cdot\mathbf{r}_{2\gamma}}. \end{aligned} \tag{3.18}$$

In the convolution term, the orientational dependence of c^{UV} on the Ω_3 is factored out in $e^{-i\mathbf{k}\cdot\mathbf{r}_{3\alpha}}$ permits integrating over the orientation of the "third" particle, Ω_3, which gives the orientationally averaged, site-site correlation functions of solvent, $h_{\alpha\gamma}^{UV}$. The 3D solute-solvent RISM equation at infinite dilution writes in reciprocal space as

$$h_\gamma^{UV}(\mathbf{k}) = \tilde{c}_\alpha^{UV}(\mathbf{k})\omega_{\alpha\gamma}(k) + \rho^V\tilde{c}_\alpha^{UV}(\mathbf{k})h_{\alpha\gamma}^{VV}(k), \tag{3.19}$$

where summation over repeating indices is implied.

Averaging the 6D solvent-solvent OZ equation (3.8) over both orientations Ω_1 and Ω_2 gives the 1D-RISM equation for radial site-site correlation functions of pure solvent,

$$\begin{aligned} h_{\alpha\gamma}^{VV}(k) &= \omega_{\alpha\mu}(k)\tilde{c}_{\mu\nu}^{VV}(\mathbf{k})\omega_{\nu\gamma}(k) \\ &\quad +\rho^V\omega_{\alpha\mu}(k)\tilde{c}_{\mu\nu}^{VV}h_{\nu\gamma}^{VV}(k), \end{aligned} \tag{3.20}$$

which produces the solvent site-site correlation function, $h_{\alpha\gamma}^{VV}$, serving as input to the 3D-RISM equation (3.19).

3.2.2 The Kirkwood-Buff Theory Combined with the Three-dimensional RISM Theory

Within the Kirkwood-Buff theory combined with 1D-RISM integral equation approach, the PMV of the solute molecule in molecular solvent, $\bar{V}_u^0$, is expressed in terms of the solute-solvent DCF's by the relation,[34)]

$$\bar{V}_u^0 = k_BT\chi_T^0\left(1-\rho^v\sum_{\alpha\gamma}\tilde{c}_{\alpha\gamma}^{uv}(k=0)\right), \tag{3.21}$$

where $\tilde{c}_{\alpha\gamma}^{uv}(k)$ is the solute-solvent site-site DCF in reciprocal space, α and γ specify interaction sites of solute and solvent molecules denoted with superscripts "U" and "V",

respectively, ρ^v is the solvent number density, T is the temperature and k_B is the Boltzmann constant, and χ_T^0 is the isothermal compressibility of pure solvent which is obtained from the site-site DCF's of pure solvent, $\tilde{c}^{vv}_{\gamma\gamma'}(k)$, in the form

$$k_B T \chi_T^0 = \left(1 - \rho^v \sum_{\gamma\gamma'} \tilde{c}^{vv}_{\gamma\gamma'}(k=0) \right)^{-1} . \tag{3.22}$$

Both the solute-solvent and solvent-solvent DCF's are calculated by solving the standard 1D-RISM integral equations with the site-site analogue of the hypernetted chain (HNC) closures.[37-40]

In this work, the KB theory is extended to the 3D-RISM description which yields 3D correlation functions of solvent interaction sites around a solute particle of arbitrary shape. The derivation of Eq. (3.21) presented in the reference.[34] is readily extended to the 3D-RISM case, resulting in the straightforward generalization

$$\bar{V}_u^0 = k_B T \chi_T^0 \left(1 - \rho_v \sum_{\gamma} \tilde{c}^{uv}_{\gamma}(\mathbf{k}=0) \right), \tag{3.23}$$

where $\tilde{c}^{uv}_{\gamma}(\mathbf{k})$ is the 3D solute-solvent site DCF in reciprocal space, and the summation is now performed only over solvent interaction sites since the solute molecule is described as a whole at the 3D level.

The 3D-RISM integral equation for the 3D solute-solvent site total and direct correlation functions, $h^{uv}_{\gamma}(\mathbf{r})$ and $c^{uv}_{\gamma}(\mathbf{r})$, is written as[42-45]

$$h^{uv}_{\gamma}(\mathbf{r}) = c^{uv}_{\gamma'}(\mathbf{r}) * \left(\omega^{vv}_{\gamma'\gamma}(r) + \rho^v h^{vv}_{\gamma'\gamma}(r) \right), \tag{3.24}$$

where $\omega^{vv}_{\gamma'\gamma}(r) = \delta(r - l^{vv}_{\gamma'\gamma})$ is the intramolecular matrix of solvent molecules with site separations $l^{vv}_{\gamma'\gamma}$, and $*$ means convolution in direct space and summation over repeating indices. The radial site-site correlation functions of pure solvent, $h^{vv}_{\gamma'\gamma}(r)$, are obtained from the conventional 1D-RISM theory using the HNC closure modified with the dielectrically consistent bridge corrections of Perkyns and Pettitt.[52,53] It provides a proper description of the dielectric properties of solution. In the 3D-RISM context, this ensures a proper macroscopic dielectric constant of solvent around the solute.[54] The 3D solute-solvent site correlation functions are specified on a 3D linear grid in a rectangular supercell, and the convolution in (3.24) is handled by means of the 3D fast Fourier transform.

Much as in the 1D-RISM approach,[37-39] a 3D-HNC closure to the 3D-RISM equation (3.24) can be constructed[41-45] similarly to the HNC approximation in integral equation theory of simple liquids.[40] In the latter case, however, it should include corrections for the supercell periodicity artifact[54] to both the direct and total 3D site correlation functions, $c_\gamma^{uv}(\mathbf{r})$ and $h_\gamma^{uv}(\mathbf{r})$, which become essentially important for a solute carrying charges. The closure thus takes the form

$$g_\gamma^{uv}(\mathbf{r}) = \exp\left(-\beta u_\gamma^{uv}(\mathbf{r}) + h_\gamma^{uv}(\mathbf{r}) - c_\gamma^{uv}(\mathbf{r}) - \Delta Q_\gamma^{uv}\right) + \Delta Q_\gamma^{uv}, \tag{3.25}$$

where $g_\gamma^{uv}(\mathbf{r}) = h_\gamma^{uv}(\mathbf{r}) + 1$ is the 3D solute-solvent site distribution function, $\beta = 1/(k_B T)$, the interaction potential $u_\gamma^{uv}(\mathbf{r})$ between solvent site γ and the whole solute is calculated on the supercell grid by using the Ewald summation method, and

$$\Delta Q_\gamma^{uv} = \frac{4\pi\beta}{V_{\mathrm{cell}}} q_0 \lim_{k\to 0} \sum_{\gamma}^{\prime} \frac{q_\alpha}{k^2} \left(\omega_{\gamma'\gamma}^{vv}(k) + \rho^v h_{\gamma'\gamma}^{vv}(k)\right), \tag{3.26}$$

is the shift in the distribution functions due to the supercell background for the solute with net charge $q_0 = \sum_\alpha q_\alpha^u$ comprising the partial site charges q_α^u.[54] The 3D solute-solvent site DCFs $c_\gamma^{uv}(\mathbf{r})$ calculated from the 3D-RISM equation (3.24) with the closure (3.25) must be corrected by subtracting the long-range electrostatic asymptotics of the periodic potential $u_\gamma^{uv}(\mathbf{r})$ synthesized by the Ewald summation, and adding back that of the single, non-periodic solute simply tabulated on the 3D-grid within the supercell.[54]

For the pair potentials between interaction sites of every species, the common model that consists of the Lennard-Jones (LJ) and electrostatic interaction terms, which is just as mentioned in the previous chapter.

The 3D-RISM/HNC equations were solved on a grid of 128^3 points in a cubic supercell of size 32 Å. To converge the equations, the modified direct inversion in the iterative subspace (MDIIS) method were used.[55,56,54]

3.3 The Partial Molar Volume of Amino Acids and Polypeptides

3.3.1 The Partial Molar Volume of Amino Acids

At first, the KB and 3D-RISM/HNC theory was tested by calculating the PMV for 20 amino acids which are classified into five categories in the conventional manner: aliphatic, nonpolar, aromatic, polar, and charged (Figure 3.1). The PMVs of the 20 amino acids in the zwitterionic form are listed in Table 3.1, along with the corresponding experimental data.[61-63] Also shown for comparison are the theoretical results obtained previously from the 1D-RISM method.[34] As is evident from Table 3.1, the results from the 3D-RISM method are in much better agreement with the experimental data than those from the 1D-RISM approach. Figure 3.4 also provides visualization by plotting the theoretical values of the PMV of the 20 amino acids against the corresponding experimental data (solid line). As seen in the figure, the results from the 3D-RISM show a remarkable correlation with experiment, whereas the 1D-RISM underestimates the PMV significantly. There remains some discrepancy between the 3D-RISM predictions and the experimental results. The most conspicuous deviation from experiment is seen in the amino acids with larger residues, where the theoretical results tend to underestimate the PMV, which becomes more pronounced with the residue size.

TABLE 3.1: Partial molar volumes (cm^3/mol) of the 20 amino acids in zwitterionic form in aqueous solutions.

	MW[a]	"1D RISM"[b]	"3D RISM"	expt.
"aliphatic"				
Ala	89.10	50.3	63.9	60.5[c]
Val	117.15	63.8	90.6	90.8[c]
Leu	131.17	73.7	105.5	107.8[c]
Ile	131.17	72.0	104.6	105.7[c]
"nonpolar"				
Gly	75.07	40.4	48.8	43.2[c]
Pro	115.13	61.5	84.7	82.5[c]
Cys	121.16	59.2	74.3	73.4[c]
Met	149.21	82.7	106.9	104.8[b]
"aromatic"				
His	155.16	71.1	94.9	98.9[e]
Phe	165.25	84.0	111.8	121.5[c]
Tyr	181.24	84.7	113.1	124.3[c]
Trp	204.27	90.5	123.9	143.4[c]
"polar"				
Asn	132.12	58.2	76.8	77.3[e]
Gln	146.15	69.2	93.5	93.6[e]
Ser	105.10	52.6	66.5	60.6[f]
Thr	119.12	59.7	81.9	76.9[f]
"charged"				
Lys	147.20	83.4	115.5	108.5[d]
Arg	175.23	84.8	123.6	127.3[d]
Asp	132.10	58.9	69.0	73.8[d]
Glu	146.12	68.1	82.9	85.9[d]

[a]molecular weight (g/mol)

[b]Ref. 34.[c]Ref. 62. [d]Ref. 18. [e]Ref. 63. [f]Ref. 47.

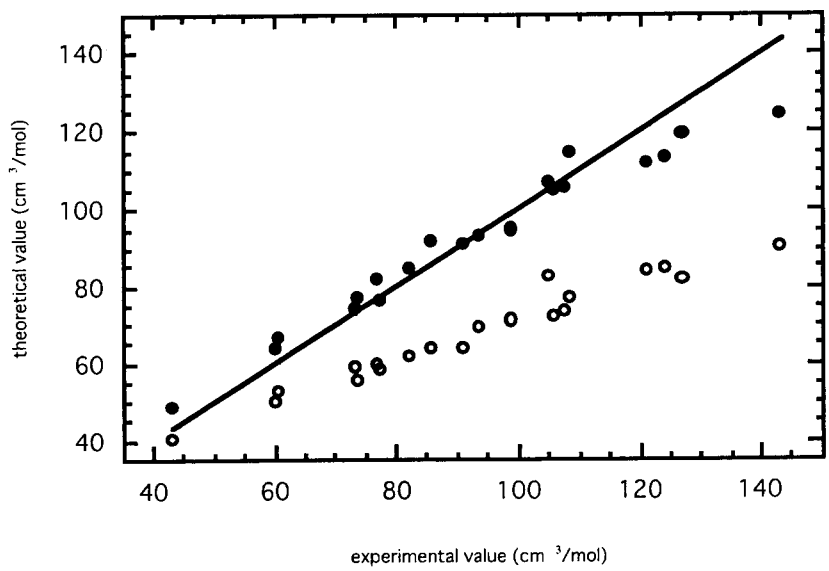

Figure 3.4: The theoretical results for partial molar volumes of amino acids against the corresponding experimental data; 3D-RISM (•), 1D-RISM (○).

In order to examine the volumetric characteristics of the amino acids according to their classification, the PMV values from experiment and the 3D-RISM theory are depicted in Figures 3.5(A) and (B), respectively, against the molecular weight of the 20 amino acids classified into the five categories. As a guide to the standard dependence of the volume upon molecular weight, the least square fitting line (LSF) for all the amino acids is drawn in both the figures. A remarkable resemblance can be observed between the theoretical and experimental results: the PMVs of amino acids in the charged group deviate from the LSF line in negative direction, while those in the aliphatic group show positive deviation, and so on. The close resemblance between the two figures reveals capability of the present theoretical method to account for the chemical specificity of amino acids in solvation. The difference between the experimental and theoretical results for the amino acids in each classification group are more closely examined. As aliphatic, nonpolar, and polar groups are concerned, the agreement between theoretical and experimental results is excellent,

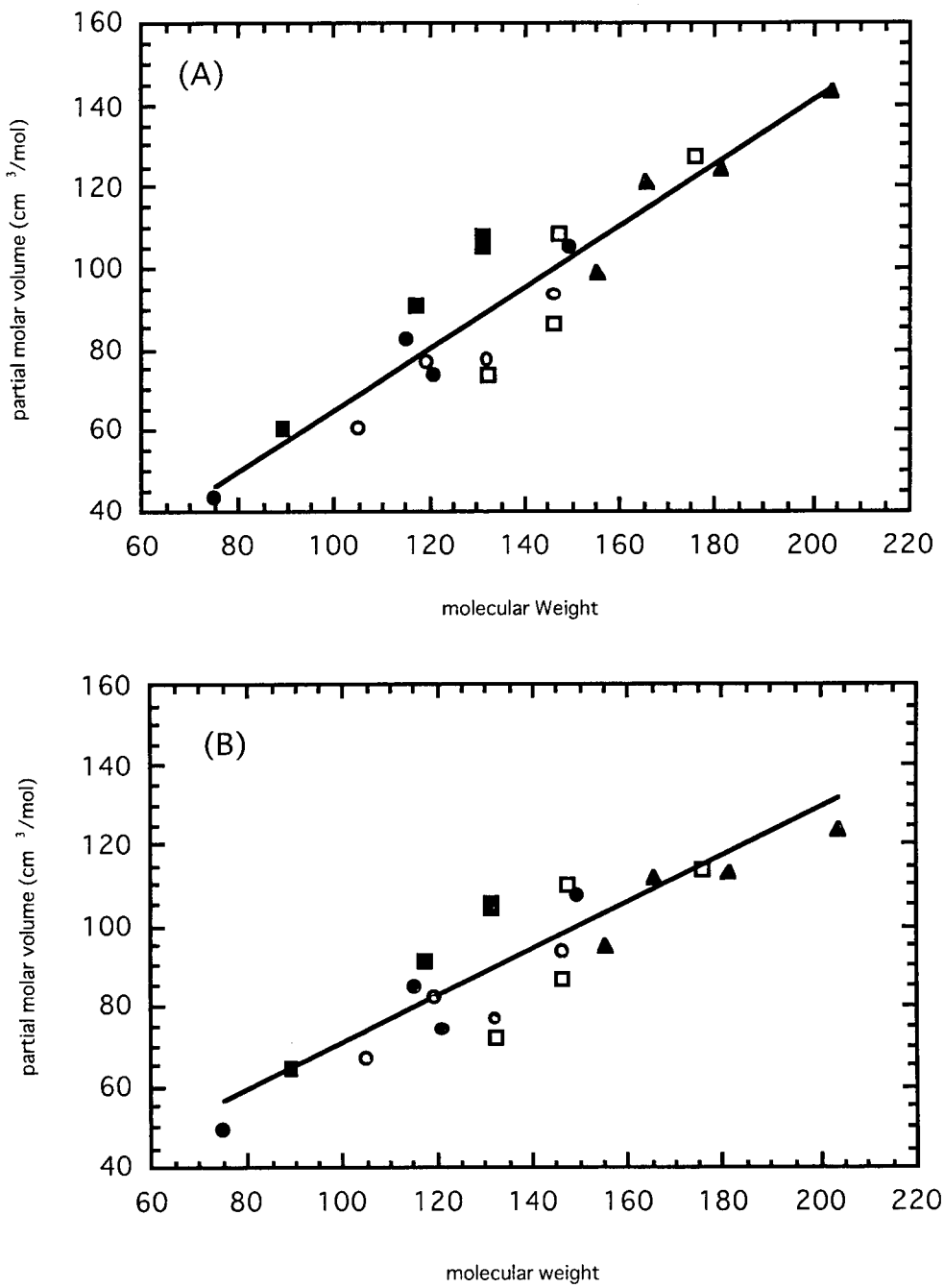

Figure 3.5: Partial molar volumes of amino acids against its molecular weight; the experiment (A) and the 3D-RISM result (B). (■); "aliphatic", (•); "nonpolar", (▲); "aromatic", (○); "polar", (□); "charged".

considering that no adjustable parameters are involved in the theoretical calculations. The small errors can be attributed both to the use of improper energy parameters and to conformational variety of those molecules in solution studied in experiment.

The 3D-RISM method significantly underestimates the PMV of all amino acids belonging to the aromatic group. It should be noted that most of the amino acids in this group are larger compared to those in the other groups, and they are the ones that have exhibited systematic negative deviation from the experiments as in Figure 3.4. Three different causes are responsible for the errors. The first is the energy parameters employed in the study, which may be too crude for describing the aromatic compounds. The other two are related to the conformational variations of the amino acids, which are not taken into account in the present study. The conformational variation of the amino acids contributes to the PMV in two different ways. One is through solute-solvent interactions, and the other through the "ideal fluctuation volume". Our calculation assumes that the amino acids are in the extended (all *trans*) conformation, which give rise to almost maximum estimates for the exclusion volume. On the other hand, our estimates for the ideal fluctuation volume is minimum, namely $\chi k_B T$. The "ideal fluctuation volume" has been introduced in the study based on the 1D-RISM theory. The ideal fluctuation volume is the volume associated with the introduction of the ideal gas into solvent. The contribution should be $\chi k_B T$ if the solute molecule is completely rigid, and $N_a \chi k_B T$ if it consists of N_a "free" atoms. In reality, a solute molecule is neither completely rigid nor free, thereby, the contribution should take a value in between $\chi k_B T$ and $N_a \chi k_B T$. It is obvious from the viewpoint of degrees of freedom that the ideal fluctuation volume in general increases with the molecule size. Plotted in Figure 3.6 is the difference of the PMV, $\Delta\bar{V}(=\bar{V}_{exp}-\bar{V}_{th})$, between the experimental ($\bar{V}_{exp}$) and theoretical results ($\bar{V}_{th}$). The maximum estimate, $N_a \chi k_B T$, for the ideal fluctuation volume is also shown by the solid line. In the case of the 1D-RISM, the difference $\Delta\bar{V}$ unphysically exceeds the maximum estimates, indicating that $\Delta\bar{V}$ includes not only the contribution from the ideal fluctuation volume but also errors of the method. In contrast, $\Delta\bar{V}$ from the 3D-RISM approach is far below the maximum estimate of the ideal fluctuation volume, which sounds more physically reliable. It is not conclusive at the moment which of the three causes is mainly responsible for the

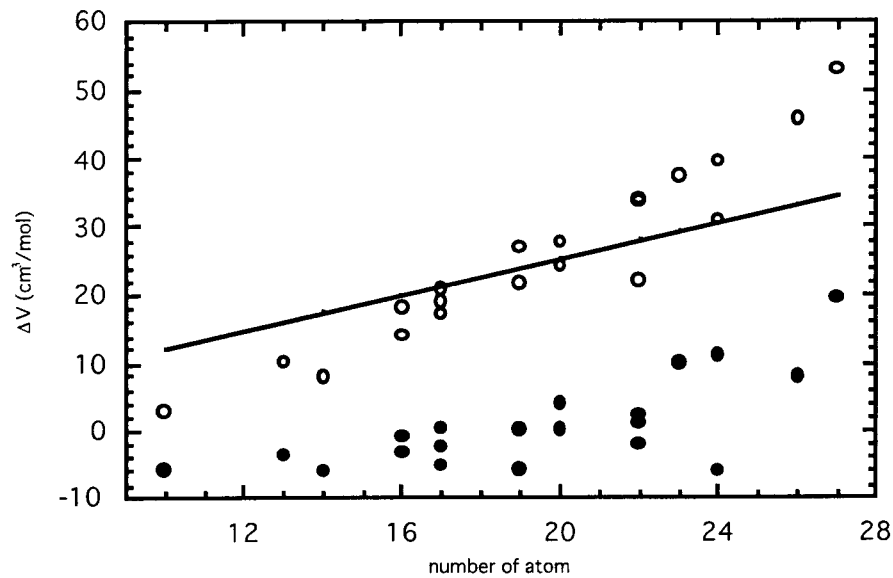

Figure 3.6: The relationship of ΔV to the number of atomic sites of amino acids. The results from the 3D-RISM (•) and the 1D-RISM (○).

underestimate of the PMV in the aromatic group.

3.3.2 The Volume Change of Polypetides Accompanied with the Helix-Coil Transition

Furthermore, the 3D-RISM approach were applied to the PMV change in the helix-coil transition of an oligopeptide. (In Figure 3.3, the molecular model of polyglutamate are shown.) According to the experiment by Noguchi and Yang,[64] the PMV is larger in the α-helix form than in the random-coil one. Namely, the PMV difference between the two forms of poly-glutamic acid ($\bar{V}_{helix} - \bar{V}_{coil}$) is about $+1.0\ cm^3/mol$ per amino acid residue. In Figure 3.8(A), the PMVs of poly-glutamic acid in an extended form and those in the α-helix are plotted against the number of amino acid residues. As can be seen, the PMV increases almost linearly with the number of residues in both the forms, but is always greater for the α-helix than for the extended conformation. The result is in qualitative

accord with the experiment. The volume difference per amino acid residue between the two forms amounts to 4.7 cm^3/mol, which apparently overestimates the experimental results. There are several reasons for the discrepancy. Salt is added to the solvent in the experiment, which is neglected in the present theoretical calculation. The random coil takes various conformations resulting in different volume, whereas we consider just one of the possible extended forms. Such conformational variety of the random coil makes contribution to the ideal fluctuation volume, which will diminish the PMV difference between the two forms. Nevertheless, even though just qualitative at the moment, the success of the 3D-RISM method is encouraging when considering that 1D-RISM approach fails to reproduce these results. Figure 3.8(B) plots the 1D-RISM predictions for the PMV of poly-glutamic acid in the extended and α-helical forms against the number of amino acid residues. The PMV of the extended form increases linearly with the number of residues, whereas that of the α-helical form turns to decrease for the peptide with more than four residues. The volume difference between the two states of the larger oligopeptide is thus predicted incorrectly, with the sign opposite to the experiment. This defies even an intuitive consideration for the volume of component amino acids sequentially added when enlarging the peptide cannot be negative. Taking into account that the α-helix makes a complete turn with 3.6 residues, this result suggests that the 1D-RISM gets in trouble when different pieces of the solute molecule are in contact and an inaccessible part for solvent molecules increases.

3.3.3 The Validity of the Three-dimensional RISM Theory for Macromolecules

It is worthwhile to provide some reasoning why the 3D-RISM/HNC method is successful for the PMV of large complex molecules while the 1D-RISM/HNC is not. The RISM theory performs orientational reduction of the 6D molecular OZ equation to operate with substantially simpler, radial site-site correlations. A basic assumption of the RISM theory implies that the DCF's between molecules can be decomposed into the additive site-site contributions, similarly to the interaction potential which constitutes its long-range asymptotics.[41,44] Being very good and reasonable for the long-range part of the DCF,

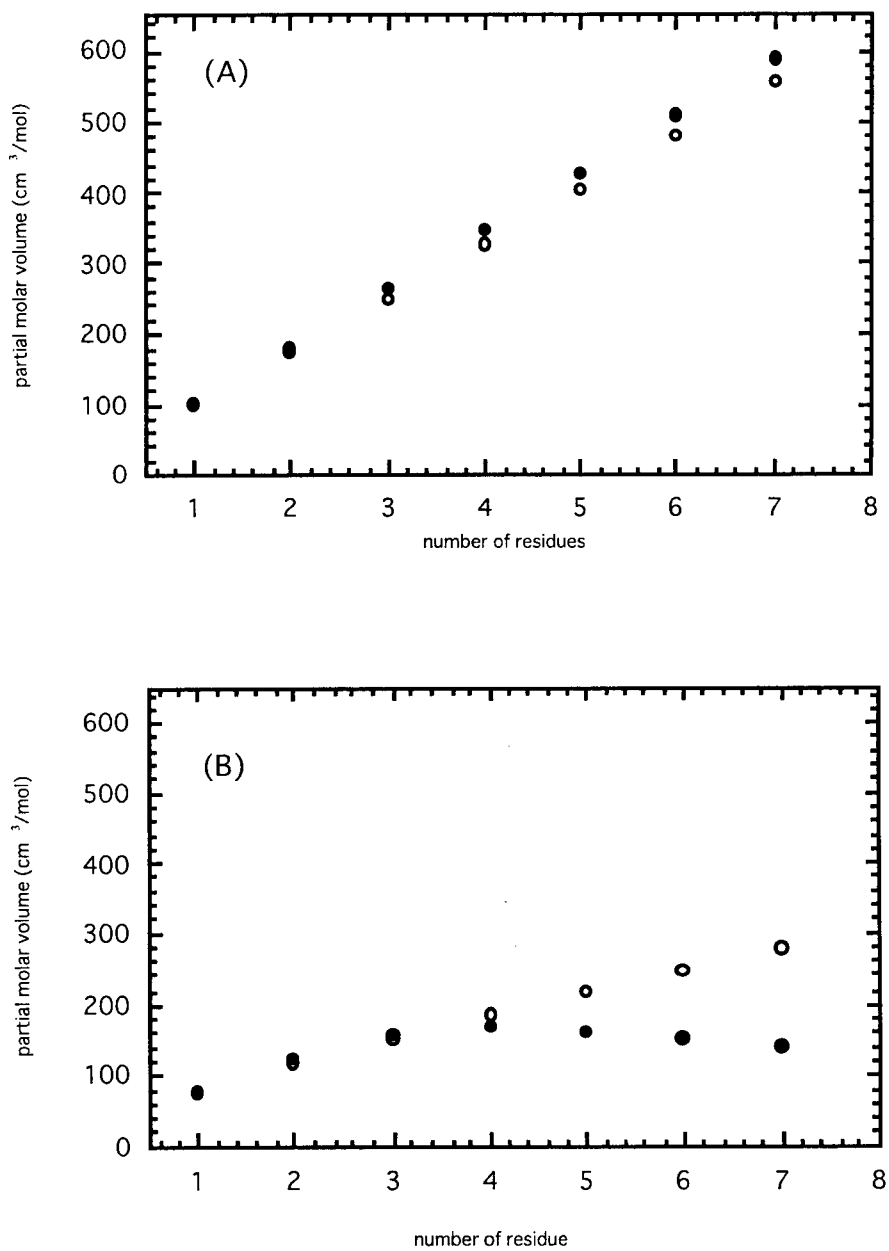

Figure 3.7: The residue dependence of partial molar volume of polyglutamate in the α-helix ($\bullet$) and the extended form ($\circ$). The results from the 3D-RISM (A) and the 1D-RISM (B).

this approximation, however, becomes essentially worse at short range in the region of the molecular repulsive core. Since no special corrections are introduces to the site-site HNC closure, this constitutes a well-documented drawback of the 1D-RISM/HNC theory which includes improper diagrams in expansions for the site-site correlations.[40] As a consequence, it mistreats the excluded volume for molecules of a large and bulky shape comprising many interaction sites with overlapping repulsive cores. One of the manifestations of that is also known as the so-called problem of auxiliary sites which label a point on the molecule but add nothing to the interaction potential.[40] As distinct, the 3D-RISM approach performs orientational averaging only for solvent molecules, keeping full description of the shape and orientation of the solute. It is thus free from the RISM artifacts "on the solute side" of the description and valid for macromolecules such as proteins at the present. One should also note that, although an entirely consistent improvement of the RISM theory is problematic,[40] it can be essentially enhanced by introducing bridge corrections, as it has been done for the hydration chemical potential of inert gases and alkanes,[57,58] organic molecules,[59] and protein.[60] Similar corrections could be elaborated for the 1D- as well as the 3D-RISM theory to improve the description of the PMV of macromolecules in solution.

3.3.4 Conclusion

In this study, the partial molar volume (PMV) of 20 amino acids in aqueous solution were calculated by using the method based on the Kirkwood-Buff (KB) theory coupled with the three-dimensional reference interaction site model (3D-RISM) integral equation method in the hypernetted chain approximation (HNC). The results are in good agreement with experimental data, and show a great improvement as compared to the conventional, one-dimensional (1D) RISM approach. However, the PMV of relatively large amino acids belonging to the aromatic group are underestimated too. This can be attributed to the effect of flexibility of solute molecules, which is neglected in the present approach treating them as rigid. Such a contribution introduced as an "ideal fluctuation volume" cannot be ignored as it becomes larger with size of the solute molecule.

Furthermore, by employing the KB and 3D-RISM approach, the PMV of the α-helical

versus extended conformations of polypeptides consisting of glutamic acids were calculated. The result for the PMV change in the conformational transition is in good qualitative agreement with the experimental results. This favorably compares to the predictions of the conventional, 1D-RISM/HNC theory giving a decrease in the PMV for the α-helix polypeptide with the backbone making a complete turn. The latter is obviously caused by the drawbacks of the 1D-RISM/HNC approach in treating the excluded volume effects. It is thus concluded that the KB and 3D-RISM/HNC integral equation method is successful and appropriate to describe the PMV of such macromolecules as polypeptides and proteins in solution, which is the sensitive property especially to size and shape of the solute molecule.

Since the method calculating the PMV has been established, further analysis will be available. The PMV are conventionally analyzed by decomposing them into five contributions: the ideal volume, the van der Waals volume, the void volume, the thermal volume, and the interaction volume. The previous experimental study provided rough molecular picture of the volume change accompanying unfolding of a protein. The picture is, however, not completed, because the volume contributions, especially the thermal volume, and the interaction volume, are not strictly determined by experimental or empirical approaches. We will redefine the volume contributions strictly by an atom-based theoretical approach.

For the biochemistry or the structural biology, it must be the final goal to explore the relation between protein conformations and biological functions. The first important step toward the goal would be to explain the conformational stability of biomolecules in terms of the microscopic structure of the molecules in solvent. It is an extremely difficult problem by any means due to the huge degrees of freedom to be handled when including protein and solvent molecules. The extended RISM method has potential capability of overcoming the problem in the level of microscopic description based on the pair correlation functions. Combined with moleculer simulations such as the Monte Carlo method, the KB and 3D-RISM/HNC integral equation method will provide a molecular picture of pressure effects on a protein structure. If we can follow up the conformations of a protein with the smallest PMV, the pressure-induced unfolding at least will be able to be traced.

Bibliography

[1] Watson, J. D., Hopkins, N. H., Roberts, J. W. Steitz, J. A., and Weiner, A. M. *Molecular Biology of the Gene*, 4th ed., W. A. Benjamin, Menlo Park, C.A. (1987).

[2] J. S. Fruton, *Molecules of Life*, John Wiley & Sons, New York, (1972).

[3] C. B. Anfinsen, *Science*, **181**, 223 (1973).

[4] IUPAC-IUB, *Biochemistry*, **9**, 3471 (1970).

[5] C. R. Cantor and P. R. Schimmel, "Biophysical Chemistry Part I: the conformation of biological macromolecules" (W. H. Freeman & Company, New York, 1980).

[6] W. Kauzmann, *Adv. Protein Chem.*, **14**, 1 (1959).

[7] P. L. Privalov, *Crit. Rev. Biochem. Mol. Biol.*, **25**, 281, (1990).

[8] R. Jaenicke, *Annu. Rev. Biophys. Bioeng.*, **10**, 1 (1981).

[9] R. Hermanns, *Annu. Rev. Biophys. Bioeng.*, **11**, 1 (1982).

[10] Y. Kuroda, S. Kidokoro, and A. Wada, *J. Mol. Biol.*, **232**, 1139 (1992).

[11] A. Tamura, et. al. *Biochemistry*, **30**, 11307 (1991)

[12] P. W. Bridgman, *J. Biol. Chem.*, **19**, 511 (1914).

[13] V.V. Mozhaev, K. Heremans, J. Frank, P. Masson, and C. Balny, *PROTEINS: Structure, Function, and Genetics*, **24**, 81 (1996).

[14] J. Jonas and A. Jonas *Annu. Rev. Biophys. Biomol. Struct.*, **23**, 287 (1994).

[15] W. Kauzmann, *Nature*, **325**, 763 (1987).

[16] J. F. Brandts in *Structure and Stability of Biological Macromolecules*, edited by S. M. Timasheff and G. D. Fasman (Marcell Deckker, New York, 1969), p. 213.

[17] F. J. Millero, *Chem. Rev.*, **71**, 147 (1971).

[18] A. A. Zamyatnin, *Ann. Rev. Biophys. Bioeng.*, **13**, 145 (1984).

[19] J. T. Edsall, *Proteins, Amino Acids and Peptides*, edited by E. J. Cohn, J. T. Edsall (Reinhold, New York, 1943), p. 155.

[20] F. J. Millero, A. L. Surdo, and C. Shin, *J. Phys. Chem.*, **82**, 784 (1978).

[21] F. Hirata and K. Arakawa, *Bull. Chem. Soc. Jpn.*, **46**, 3367 (1973).

[22] Y. Yoshimura and M. Nakahara, *J. Chem. Phys.*, **81**, 4080 (1984).

[23] P. G. Kusalik and G. N. Patey, *J. Chem. Phys.*, **86**, 5115 (1987).

[24] P. G. Kusalik and G. N. Patey, *J. Chem. Phys.*, **88**, 7715 (1988).

[25] P. G. Kusalik and G. N. Patey, *J. Chem. Phys.*, **89**, 5843 (1988).

[26] M. Ohba, F. Kawaizumi, and H. Nomura, *J. Phys. Chem.*, **96**, 5129 (1992).

[27] S. Chong and F. Hirata, *J. Phys. Chem. B*, **101**, 3209 (1997).

[28] N. Matubayasi and R. M. Levy, *J. Phys. Chem.*, **100**, 2681 (1995).

[29] D. M. Lockwood and P. J. Rossky, *J. Phys. Chem. B*, **103**, 1982 (1999).

[30] F. Hirata, T. Imai, and M. Irisa, *Rev. High Pressure Sci. Tech.*, **8**, 96 (1998).

[31] M. Irisa, K. Nagayama, and F. Hirata, *Chem. Phys. Lett.*, **207**, 430 (1993).

[32] M. Irisa, K. Takahashi, K. Nagayama, and F. Hirata, *Mol. Phys.*, **85**, 1227 (1995).

[33] J. G. Kirkwood and F. P. Buff, *J. Chem. Phys.*, **19**, 774 (1951).

[34] T. Imai, M. Kinoshita, and F. Hirata, *J. Chem. Phys.*, **112**, 9469 (2000).

[35] D. Chandler and H.C. Andersen, J. Chem. Phys. **57**, 1930 (1972).

[36] D. Chandler, *J. Chem. Phys.*, **59**, 2749 (1973).

[37] F. Hirata and P. J. Rossky, *Chem. Phys. Lett.*, **83**, 329 (1981)

[38] F. Hirata, B. M. Pettit, and P. J. Rossky *J. Chem. Phys.*, **77**, 509, (1982)

[39] F. Hirata, P. J. Rossky, and B. M. Pettit, *J. Chem. Phys.*, **78**, 4113, (1983)

[40] J. P. Hansen and I. R. McDonald, *Theory of Simple Liquids*, 2nd edn. (Academic, London, 1986).

[41] C. M. Cortis, P. J. Rossky, and R. A. Friesner, *J. Chem. Phys.*, **107**, 6400 (1997).

[42] D. Beglov and B. Roux, *J. Phys. Chem. B*, **101**, 7821 (1997).

[43] A. Kovalenko and F. Hirata, *Chem. Phys. Lett.*, **290**, 237 (1998)

[44] A. Kovalenko and F. Hirata, *J. Chem. Phys.*, **110**, 10095 (1999)

[45] A. Kovalenko and F. Hirata, *J. Chem. Phys.*, **112**, 10391 (2000)

[46] M. Kikuchi, M. Sakurai, and K. Nitta, *J. Chem. Eng. Data*, **40**, 935 (1995).

[47] M. Mizuguchi, M. Sakurai, and K. Nitta, *J. Solution Chem.*, **26**, 579 (1997).

[48] Y. Yasuda, N. Tochio, M. Sakurai, and K. Nitta, *J. Chem. Eng. Data*, **43**, 205 (1998).

[49] D. Beglov and B. Roux, *J. Chem. Phys.*, **103**, 360, (1995).

[50] D. Beglov and B. Roux, *J. Chem. Phys.*, **104**, 8678, (1996).

[51] M. Ikeguchi and J. Doi, *J. Chem. Phys.*, **103**, 360, (1995).

[52] J. S. Perkyns and B. M. Pettitt, *Chem. Phys. Lett.*, **190**, 626 (1992).

[53] J. S. Perkyns and B. M. Pettitt, *J. Chem. Phys.*, **97**, 7656 (1992).

[54] A. Kovalenko and F. Hirata, *J. Chem. Phys.*, **112**, 10403 (2000).

[55] A. Kovalenko, S. Ten-no, and F. Hirata, *J. Comput. Chem.*, **20**, 928 (1999).

[56] A. Kovalenko and F. Hirata, *J. Phys. Chem. B*, **103**, 7942 (1999).

[57] L. Lue and D. Blankschtein, *J. Phys. Chem.*, **96**, 8582 (1992).

[58] A. Kovalenko and F. Hirata, *J. Chem. Phys.*, **113**, 2793 (2000).

[59] Q. Du, D. Beglov, and B. Roux, *J. Phys. Chem. B*, **104**, 796 (2000).

[60] A. Kovalenko and F. Hirata, and M. Kinoshita, *J. Chem. Phys.*, **113**, 9830 (2000).

[61] M. Kikuchi, M. Sakurai, and K. Nitta, *J. Chem. Eng. Data*, **40**, 935 (1995).

[62] M. Kikuchi, M. Sakurai, and K. Nitta, *J. Solution Chem.*, **26**, 579 (1997)

[63] Y. Yasuda, N. Tochio, M. Sakurai, and K. Nitta, *J. Chem. Eng. Data*, **43**, 205 (1998).

[64] H. Noguchi, J. S. Yang, *Biopolymers*, **1**, 359-370 (1963).

Acknowledgment

The author would like to acknowledge the continuous guidance and encouragement of Prof. Kazuyuki Akasaka and Prof. Fumio Hirata (Institute for Molecular Science). The author is grateful to Dr. Andriy Kovalenko and Dr. Hirofumi Sato (Institute for Molecular Science) for their help and joint work. The author would also thank Dr. Imai (Institute for Molecular Science) for his support with computational technics.

This work was supported by the grant from the Ministry of Education, Science, Sports and Culture (MONBUSHO) of Japan.

Finally the author has enjoyed the comradeship and useful discussion from Dr. Ryo Akiyama (Cornell Univ., U.S.A) and members in the laboratory of theoretical group in Institute for Molecular Science.

Publication List

Chapter2

Y. Harano, H. Sato, and F. Hirata, *J. Am. Chem. Soc.*, **122**, 2289-2293 (2000).

Y. Harano, H. Sato, and F. Hirata, *Chem. Phys.*, **258**, 151-161 (2000).

Chapter3

Y. Harano, T. Imai, A. Kovalenko, M. Kinoshita, and F. Hirata, *J. Chem. Phys.*, submitted.